

REVIEW

Challenges and opportunities for graphene as transparent conductors in optoelectronics



Yi Song, Wenjing Fang, Roberto Brenes, Jing Kong*

Department of Electrical Engineering and Computer Sciences, Massachusetts Institute of Technology, Cambridge, MA 02139, USA

Received 22 June 2015; received in revised form 26 October 2015; accepted 13 November 2015
Available online 21 December 2015

KEYWORDS

Graphene;
Transparent conductor;
Optoelectronic devices;
Solar cells;
LEDs

Summary As optoelectronic devices become more ubiquitous and applications for such devices begin to diversify, there is an increasing demand for an alternative transparent conducting film to address the shortcomings of transparent metal oxides. Graphene, which combines excellent optical transparency with mechanical robustness and chemical inertness, is a strong candidate for this purpose. Synthesize techniques such as chemical vapor deposition and liquid phase exfoliation allows researchers to produce large-area transparent conducting films that can be used for devices such as solar cells and light-emitted diodes. However, practical issues such as insufficient conductivity or surface roughness from transfer often hamper device performance. Nonetheless, researchers have succeeded in demonstrating graphene electrode-based solar cells, LEDs, photodetectors, and lasers. In this review, we present an overview of progress made in building optoelectronic devices with graphene as the transparent conductor and identify the major challenges that must be overcome before the material can move from the laboratory to industry.

© 2015 Elsevier Ltd. All rights reserved.

Introduction and background

Graphene is a two-dimensional array of carbon atoms arranged in a planar hexagonal configuration. Over the past decade, the material has attracted enormous attention

from researchers due to its remarkable physical and chemical characteristics. From an optoelectronics standpoint, graphene is both electrically conductive and optically transparent – a pair of properties rarely found together – making it a natural candidate for next-generation transparent conductors (TCs). Currently the TC market is dominated by conductive metal oxides such as indium tin oxide (ITO), fluorine-doped tin oxide (FTO), and aluminum-doped zinc oxide (AZO). Of these, ITO offers the best conductivity. However, it has the drawback of being expensive because indium

* Corresponding author. Tel.: +1 617 324 4068.
E-mail address: jingkong@mit.edu (J. Kong).

is a rare earth metal primarily found in zinc deposits and is therefore produced in small quantities as a by-product. To address increasing demand, researchers have been exploring the possibility of applying other materials such as metal grids/nanowires, carbon nanotubes (CNTs), conductive polymers, and graphene.

All of the emerging technologies listed above have potential advantages over ITO in certain respects such as conductivity, flexibility, or cost. Metal grids offer excellent conductivity and good optical transmittance but require patterning via photolithography or shadow mask evaporation. More recently, researchers developed other types of metallic networks such as spin-on silver nanowires or metallic 'nanotroughs'. Disadvantages include higher cost, greater surface roughness, instability in air due to oxidation, and hazing. We refer the reader to other review articles for detailed discussions [1–3]. Carbon nanotubes can, in some ways, be thought of as the predecessor to graphene. CNT transparent conducting films are approaching realization in industry; in fact, companies have demonstrated working touch screens using carbon nanotube films. However, synthesis and purification of high quality nanotubes can be difficult and like nanowires, nanotube films have higher surface roughness, which is undesirable for some applications [4,5]. Conducting polymers such as PEDOT:PSS have also shown promise. Normally, the conductivity of these polymers is very low compared to ITO. Simple modifications such as dipping in alcohol can enhance the conductivity significantly, but still lower than other TCs. PEDOT:PSS can also be deposited over large areas by spin-coating, printing, or oxidative chemical vapor deposition. As before, we refer to other comprehensive reviews for more information on the topic [6,7]. These emerging technologies are very different, each having advantages and disadvantages that constantly evolve as research progresses rapidly. In this review, we focus our attention on graphene.

The atomic arrangement of carbon atoms in graphene gives rise to unique electrical properties. The delocalized π -electrons have mobility values as high as $200,000 \text{ cm}^2/\text{Vs}$ at room temperature, resulting in intrinsic resistivity as low as $30 \Omega/\text{sq}$ [8]. The theoretical optical absorption of graphene – 2.3% per layer – is determined by the fine structure constant, which describes the coupling between light and relativistic electrons [9]. These theoretical values for sheet resistance and optical transmittance compare favorably to carbon nanotubes films and conductive polymers. Furthermore, graphene films are uniform with atomically flat surfaces and can be cheaper to synthesize than metal grids or nanowires. In spite of these advantages, when comparing graphene to ITO, many researchers are skeptical about graphene's prospects of becoming the dominant TC. History has shown that older, established technologies are difficult to displace, and ITO is indeed a well-entrenched industry standard. Efforts have also been made to recover indium from used electronics such as LCD panels to alleviate the resource demand [10]. However, at present, ITO has mostly been used in applications with flat, rigid substrates. Recently, bendable or curved devices have become an emerging trend, where the flexibility of graphene may play a key role. Furthermore, other advantages of graphene open possibilities for technologies that may not be compatible with ITO. For example, ITO cannot be used in dye

sensitized solar cells because the sintering process during fabrication requires the TC to survive temperatures upwards of 400°C . Similarly, in organic photovoltaic devices (OPVs), ITO has been shown to degrade over time, resulting in reduced performance and lifetime [11,12]. In contrast, graphene has remarkable thermal stability and chemical inertness, making it a promising candidate for these applications. In addition, it is anticipated there will be increased demand for TCs in the future, so the cost and abundance of graphene may become more important.

Because graphene is still a relatively new material, researchers take different approaches in trying to make it more industrially relevant. One approach is to improve the physical properties of the graphene itself. While the theoretical properties of graphene, such as its atomic flatness and high electrical conductivity, are highly attractive, it is often difficult to achieve such results in practice. Thus, much of the community's efforts focuses on making graphene more attractive by bridging the gap between theory and practice, for example: controllably synthesizing large-area defect-free films, improving the sheet resistance by surface modifications, or developing transfer processes that allows the growth substrates to be recycled. Many of these efforts are described in section 2-graphene synthesis and processing. Another approach is to use graphene for existing technologies in place of conventional TCs to assess the advantages and disadvantages of the material. For example, researchers have demonstrated flexible organic solar cells and LEDs using graphene electrodes with performance similar to or exceeding that of ITO-based devices. At this stage, these investigations are quite preliminary and many aspects such as device reliability and reproducibility have not yet been thoroughly investigated. Specific results are summarized in section 3 of this review – optoelectronic devices with graphene electrodes.

Graphene synthesis and processing

Synthesis of large-area graphene

In 2004, graphene was first isolated by mechanically exfoliating from graphite flakes – a process colloquially known as 'scotch-taping' (Fig. 1a) [13]. Unfortunately, the size of the exfoliated flakes was limited to hundreds of microns, which meant that fabricating large-scale optoelectronic devices were not possible using mechanically exfoliated graphene. However, researchers soon developed scalable methods of preparing large-area film – the most common of which are chemical vapor deposition (CVD) and liquid phase exfoliation. We briefly discuss these two methods.

Chemical vapor deposition

CVD is a bottom-up synthesis method that generally produces continuous films with sheet resistances of a few hundred Ohms per square and optical losses very close to the ideal 2.3% per layer, which makes it very popular amongst research communities. In a typical CVD process, the growth substrate (most commonly copper foil or nickel thin film) is annealed at high temperatures ($\sim 1000^\circ\text{C}$) in a reducing environment. After annealing, a carbon source such as methane is introduced into the growth chamber. The high

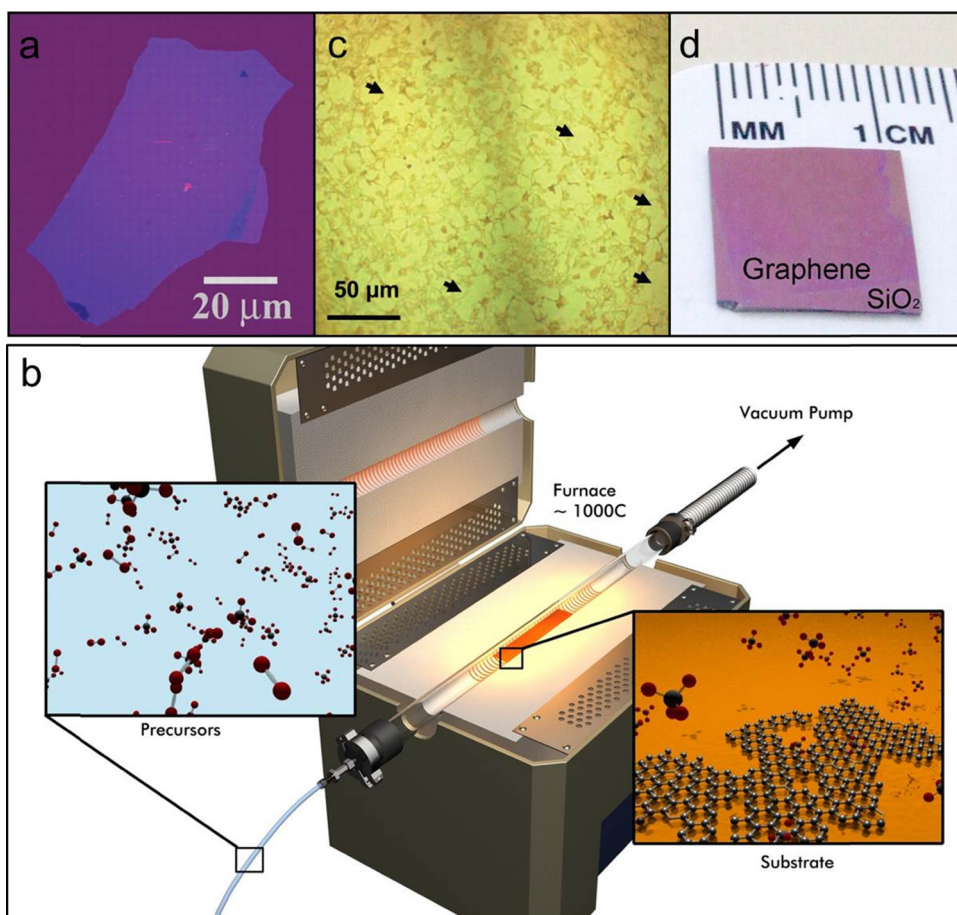


Figure 1 (a) Optical image of mechanically exfoliated graphene flake. Reprinted with permission from [13]. Copyrights 2004 American Association for the Advancement of Science. (b) Illustration of graphene synthesis by CVD. (c) Graphene synthesized on nickel thin film; arrows indicate thin monolayer regions. (d) Monolayer graphene synthesized on copper foil and transferred onto SiO₂/Si substrate. Reprinted with permission from [14]. Copyrights 2004 American Association for the Advancement of Science.

temperature coupled with the catalytic properties of the metal substrates causes the carbon to decompose and dissolve (Fig. 1b). Generally speaking, in the case of substrates with high carbon solubility, such as nickel, under most synthesis conditions the dissolved carbon precipitates when cooled down to room temperature and forms multilayer graphene on the surface (Fig. 1c). In the case substrates with low carbon solubility, such as copper, under low pressure CVD conditions, the reaction terminates when the surface of the copper is covered with graphene, resulting in monolayer graphene, as shown in Fig. 1d [14,15]. Methane is the most common precursor but researchers have shown that virtually any source of carbon, including solid carbon, can be used [16,17]. CVD-grown graphene on metal substrates is polycrystalline with domain sizes typically in the range of microns to hundreds of microns and the individual domains are stitched together to form a single continuous film. Improving the CVD process to increase the domain size is a hot area of research and some groups have already reported millimeter to centimeter-sized domains [18–20]. Wafer-scale epitaxial growth of single crystalline graphene has been demonstrated on silicon carbide [21] and, more recently, on germanium [22]. In recent years, researchers have also demonstrated continuous roll-to-roll

CVD growth, which will be necessary for industrial-scale production [23–25]. Finally, as will be discussed in detail later, the graphene must be transferred from the growth substrate to the target substrate, which is often not a trivial procedure. Because of this, there is also interest in directly synthesizing graphene on rigid substrates such as SiO₂ by precipitation from metal films [26,27]. At present, CVD appears to be favored by researchers working on optoelectronic devices because it generally produces graphene with better electrical properties compared to other large-scale synthesis methods.

Liquid phase exfoliation

Because of the throughput limitations of CVD, many researchers have explored liquid phase exfoliation as a more scalable top-down synthesis method. Graphite flakes can be mass-exfoliated into few-layer graphene in solution, which offers higher throughput suitable for industrial-scale applications. However, this comes at the expense of performance, as the graphene is not a single continuous film, but rather, a network of interconnected flakes, as can be seen in Fig. 2a. Ideally, the graphite should be broken down into large monolayer or few-layer graphene flakes. The most common approaches to liquid phase exfoliation are

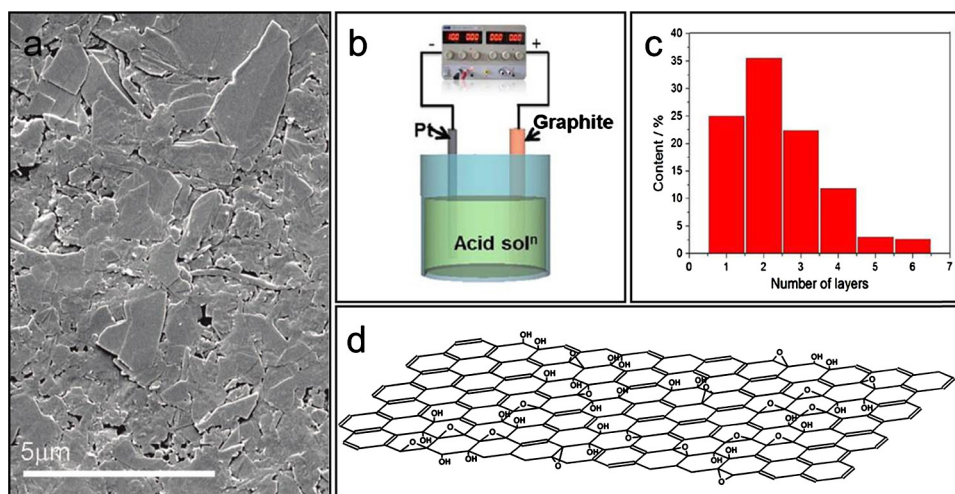


Figure 2 (a) SEM image of liquid phase exfoliated graphene exfoliated in water and surfactant. Reprinted with permission from [29]. Copyrights 2009 American Chemical Society. (b) Illustration of electrochemical exfoliation of graphite and (c) the corresponding thickness distribution. Reprinted with permission from [30]. Copyrights 2013 American Chemical Society. (d) Illustration of the structure of graphene oxide. Reprinted with permission from [36]. Copyrights 1998 Elsevier.

ultra-sonication in surfactant solutions or organic solvents [28,29], electrochemical exfoliation in electrolyte solution [30,31], and chemical reduction of exfoliated graphene oxide [32,33]. Of these techniques, the simplest is to sonicate graphite flakes in water with surfactant. As reported by Lotya et al., 40% of exfoliated flakes had fewer than 5 layers and 3% of flakes were monolayer [29]. Exfoliating in organic solvents yields similar results [28]. To achieve better monolayer yield, graphite flakes can be electrochemically exfoliated in an aqueous solution of inorganic salts [31,34]. Applying a voltage across the electrodes causes ions in the solution to intercalate between graphite layers, separating them into few-layer graphene flakes (Fig. 2b). Parvez et al. reported that 85% of electrochemically exfoliated flakes were 3 layers or less (Fig. 2c) and the hole mobility of individual flakes was measured to be $310 \text{ cm}^2/\text{Vs}$. Reduced Graphene Oxide (rGO) is another approach to liquid phase exfoliation. Graphite flakes are first oxidized using a mixture of sulfuric acid, sodium nitrate, and potassium permanganate (Hummers method) [35]. The oxidation process increases the interlayer spacing of the graphite flakes and allows the individual layers to be more easily separated via sonication or stirring, producing a suspension of GO flakes in water. The structure of GO is shown in Fig. 2d. The flakes can then be reduced by a variety of methods such as exposing to hydrazine, exposing to hydrogen plasma, or even illuminating with light from a camera flash [32,33]. Solution processed films can be sprayed or painted onto practically any surface and therefore may not require a transfer step.

Transfer

CVD graphene is grown on metal foil or thin film and so it usually needs to be transferred onto another substrate for device fabrication. Solution processed graphene can be directly deposited on the target substrate via spray or spin-casting but high temperature annealing is often necessary to reduce the sheet resistance, which limits the choice of

substrate. For heat-sensitive substrates, a common strategy is to deposit the flakes on thermally stable substrate such as SiO_2 for annealing and then transfer onto the target substrate [37]. Thus, the problem of transfer is relevant to both CVD and solution exfoliated films. The most common graphene transfer procedure is spin-coating a thin PMMA layer, etching away the growth substrate in solution, scooping the graphene/PMMA film onto the target substrate, and finally dissolving the PMMA layer [15]. This procedure is the dominant method used by researchers who work with CVD graphene and many have reported modifications to improve the quality of the transferred film. For example, it has been shown (Fig. 3a) that re-depositing a second layer of PMMA onto the graphene after scooping onto the substrate results in fewer tears and better sheet resistance [38,39]. Applying a thorough RCA cleaning process on the floating graphene/PMMA film also removes contaminants and reduces crack formation [40]. Nevertheless, there are some limitations such as wrinkles in the transferred film and polymer residues on the surface. As time progressed, there have constantly been improvements and evolutions of the original process to overcome these issues. Here, we give an overview of these findings.

After etching away the copper growth substrate, the graphene/PMMA film is left floating in water. The PMMA membrane (typically $50 \text{ nm} - 1 \mu\text{m}$) is so thin that it crumples when pulled from water so the target substrate must be immersed to scoop out the film. This is unacceptable for some devices such as organic solar cells or LEDs since many organic compounds are highly sensitive to water. To circumvent this, researchers often use a thicker transfer membrane that stays rigid when removed from water and can therefore be pressed onto the target substrate in air; this is commonly referred to as 'dry-transfer'. One option is Polydimethylsiloxane (PDMS), as demonstrated by Kim et al. (Fig. 3b) [41]. Graphene grown on nickel was attached to a PDMS stamp and pressed onto a surface; the PDMS was subsequently removed, leaving the graphene attached to the target substrate. The graphene was wrinkled after

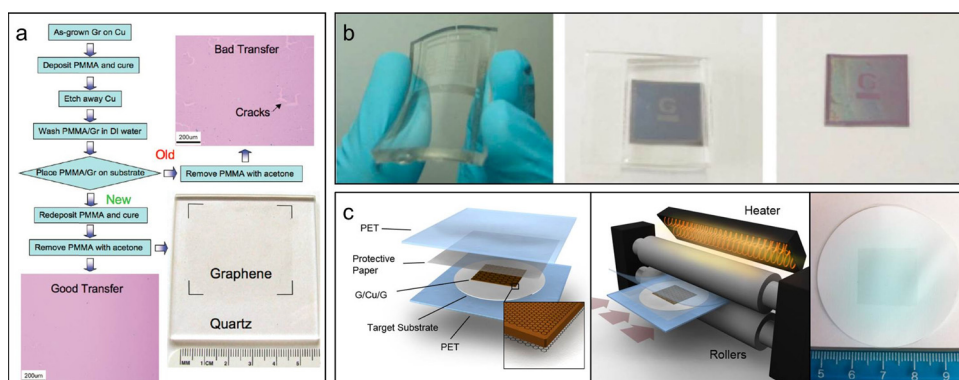


Figure 3 (a) Modified PMMA transfer procedure developed by Li et al. Reprinted with permission from [39]. Copyrights 2009 American Chemical Society. (b) Transfer of graphene grown on nickel thin film using a PDMS stamp. Reprinted with permission from [41]. Copyrights 2009 Nature Publishing Group. (c) Illustration of direct transfer process used in [44] and a photograph of graphene transfer onto a PTFE filter using this method.

transfer but the wrinkles were shown to make the film more resilient to mechanical strain. Song et al. improved this procedure by adding a 'self-release layer (SRL)' between the graphene and PDMS [42]. The adhesion between the PDMS and SRL is weaker so the adhesion between the graphene and substrate so the PDMS stamp can be removed easily. Bae et al. demonstrated a roll-to-roll 'dry transfer' method onto flexible substrates using thermal release tape as the transfer membrane [43]. Thermal release tape is attached to graphene grown on copper foil and the copper is etched away. The tape/graphene is then pressed onto PET and heated to 120 °C to release the film. However, like PMMA, thermal release tape leaves residues, which may be detrimental for devices.

Direct transfer of graphene onto flexible substrates via lamination has also been demonstrated in several reports. The general idea behind this technique is that instead of using an intermediate membrane, one can press the graphene/copper against the target substrate and etch away the copper, leaving the graphene film attached to the target substrate. As a result, the exposed side of the graphene is free of PMMA residues. Han et al. first demonstrated this transfer method by on PET; the PET was heated to 115 °C for the lamination [45]. O'Hern et al. transferred graphene onto Polycarbonate filters and TEM grids using a similar method without heating and concluded that the hydrophobicity of the target substrate is critical to ensuring a successful transfer [46]. Our group also thoroughly investigated the heated lamination transfer method on a wide variety of substrate (Fig. 3c) [44]. We concluded that the method can be generalized to any flexible substrate provided that the lamination apparatus can reach glass transition temperature of the material. A thin PMMA coating can also be applied to substrates that are too hydrophilic. Measurable sheet resistance values were obtained on all substrates investigated, which indicates that the transferred films were electrically continuous, but the range varied from 170 to 3000 Ω /sq. Parvez et al. developed a similar procedure for electrochemically exfoliated film whereby, the graphene was vacuum filtered onto a PTFE membrane and pressed against the target substrate (PET), as shown in Fig. 4a [30]. Van der Waal interactions ensured that the graphene stuck to the PET. Because these direct transfer techniques depend on close

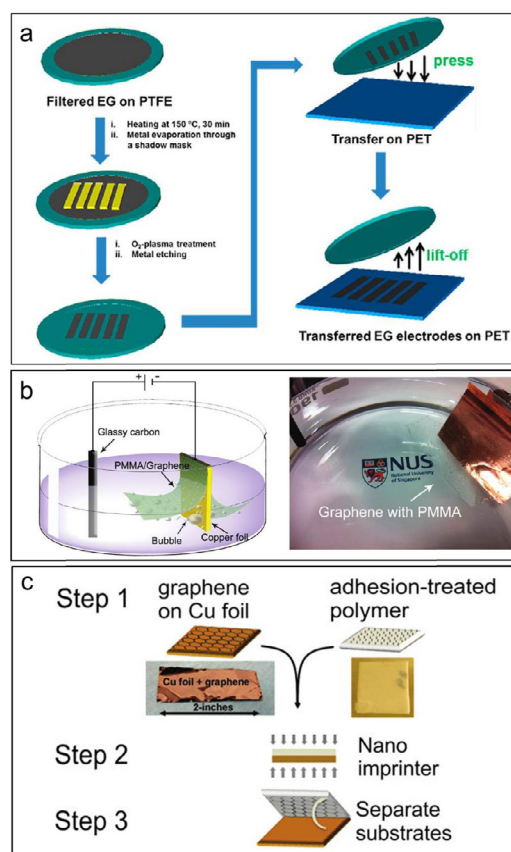


Figure 4 (a) Transfer of liquid phase exfoliated graphene from a PTFE filter to PET. Reprinted with permission from [30]. Copyrights 2013 American Chemical Society. (b) Illustration and photograph of the 'bubble transfer' procedure. Reprinted with permission from [47]. Copyright 2011 American Chemical Society. (c) Illustration of dry transfer using adhesion-treated polymer. Reprinted with permission from [48]. Copyright 2011 American Chemical Society.

contact between the graphene and target substrate, they are most effective on soft thermoplastics. At present, there does not appear to be an effective direct transfer technique for hard substrates.

The works referenced above all etch away the growth substrate during the transfer process, sacrificing $\sim 25\ \mu\text{m}$ of copper foil for a monolayer of graphene. In order to reduce the overall cost of producing CVD graphene – which is often cited as a potential advantage of graphene over ITO – it is necessary to recycle the growth substrate. Electrochemical delamination, colloquially known as ‘bubble transfer’, allows graphene to be separated from metal foils. This method was first demonstrated by Wang et al. on copper foil (Fig. 4b) [47] and soon thereafter on platinum foil by Gao et al. [49]. In both reports, PMMA is first coated on the graphene/metal. The stack is immersed in an aqueous electrolyte solution and the graphene/PMMA is delaminated by applying a voltage between the metal and a counter electrode. The metal foil can be recycled indefinitely and, in fact, becomes smoother over time. Another advantage of this method is that the graphene can be delaminated from both sides of the metal, effectively doubling the throughput. However, after the graphene is delaminated, the remainder of the procedure is identical to the standard PMMA process and is therefore subject to the same issues such as wrinkles and residues. Lock et al. demonstrated a direct-transfer method that also allows the growth substrates to be re-used [48]. Polystyrene was treated with CO_2 plasma and covered with the linker molecule *N*-ethylamino-4-azidotetrafluorobenzoate (TFPA– NH_2) by dip coating. Azides were chosen as the linker molecule because form strong covalent bonds with graphene. The graphene/copper was then pressed against the polymer substrate using a nano-imprinter at 500 psi for 30 min. Because the graphene adheres more strongly to the azide molecules than the copper foil, the polystyrene/graphene can be peeled off, leaving the copper intact. The process is illustrated in Fig. 4c. The resultant films had sheet resistances of 1–3 k Ω /sq, depending on the method of attachment between the polymer substrate and linker molecule.

Applying these transfer techniques to actual optoelectronic devices represents an exciting opportunity for future research. The majority of research on optoelectronic devices with graphene electrodes still uses the standard PMMA transfer procedure because it reliably produces higher-quality films. However, when considering industrial applications, ensuring that the transfer is scalable and can be easily automated is just as important. Much of current research regarding scaling and automation focuses on roll-to-roll processes, which is relevant to flexible substrates. For applications that use rigid substrates, scaling up transfer throughput would require an automated, wafer-scale batch transfer process. These developments will be driven by higher demand once graphene-based devices move from laboratory-scale to practical applications.

Conductivity and optical transmittance

In many cases, electrical conductivity and optical transmittance are the most important metrics for TCs. Researchers often use the DC conductivity to optical conductivity ratio ($\sigma_{\text{DC}}/\sigma_{\text{OP}}$) as a figure of merit in evaluating transparent conductors. For thin metallic films, the transmittance (T), sheet

resistance (R_s), and $\sigma_{\text{DC}}/\sigma_{\text{OP}}$ are related by the following expression:

$$T = \left(1 + \frac{188.5}{R_s} \frac{\sigma_{\text{OP}}}{\sigma_{\text{DC}}} \right)^{-2} \quad (1)$$

Because $\sigma_{\text{DC}}/\sigma_{\text{OP}}$ is difficult to measure directly, researchers often specify a sheet resistance value at a particular transmittance. A plot of sheet resistance versus optical transmittance for various values of $\sigma_{\text{DC}}/\sigma_{\text{OP}}$ is shown in Fig. 5a. ITO has $\sigma_{\text{DC}}/\sigma_{\text{OP}}$ of about 500, which corresponds to 10 Ω /sq at 93% transmittance. Parity with ITO is often seen as the ultimate goal when dealing with graphene as TCs and is seen as so important that nearly every work in the field cites the conductivity of ITO as the reference metric. Chen et al. theorized that intrinsic graphene has mobility of 200,000 cm^2/Vs at $10^{12}\ \text{cm}^{-2}$ carrier density for sheet resistance of 30 Ω /sq [8]. The 30 Ω /sq is often quoted in literature and has been experimentally verified for suspended monolayer flakes [50]. The optical transmittance of graphene is governed by the fine structure constant ($\alpha = e^2/\hbar c$), which describes the coupling between light and relativistic electrons [9]. Pristine graphene has optical absorption of $\pi\alpha = 2.3\%$ per layer. Thus, three layers of perfect graphene could potentially achieve the industrially competitive standard of 10 Ω /sq at 94% transmittance (equal to ITO) [51]. Unfortunately, large-area graphene films have numerous other sources of scattering such as defects, wrinkles, and domain boundaries. As a result, real graphene films used in devices are not nearly as conductive; the range of sheet resistance values reported in literature is 75–1000 Ω /sq for monolayer CVD graphene and 0.3–10 k Ω /sq for solution exfoliated graphene. Here, we present strategies that researchers use to enhance the conductivity of graphene films. Because they are very different, we discuss CVD graphene and liquid exfoliated graphene separately.

Conductivity of CVD graphene

Fundamentally, the sheet resistance of *N*-layer CVD graphene, assuming that the layers are independent, can be expressed as

$$R_{\text{sh}} = \left(\sum_{i=1, \dots, N} q\mu_i n_i \right)^{-1} \quad (2)$$

q is the elementary charge, μ_i is the carrier mobility of the *i*th layer and n_i is the sheet carrier concentration of the *i*th layer. From this, we can see that in order to minimize sheet resistance, we should try to increase mobility or increase carrier concentration (i.e. ‘‘dope’’ the graphene). Carrier concentration can be increased by transferring the graphene onto polar substrates such as SiO_2 , by exposing it to air, or by exposing it to highly electronegative chemicals. Graphene on SiO_2 stored in air is typically p-doped. Pristine graphene has extremely high mobility but can be reduced drastically by any defects such as point defects or holes/tears and additional sources of scattering. Thus, mobility is often indicative of the quality of the graphene film. Finally, because doping introduces charged impurities, mobility typically decreases as carrier concentration increases. Unfortunately, these parameters are not easy to

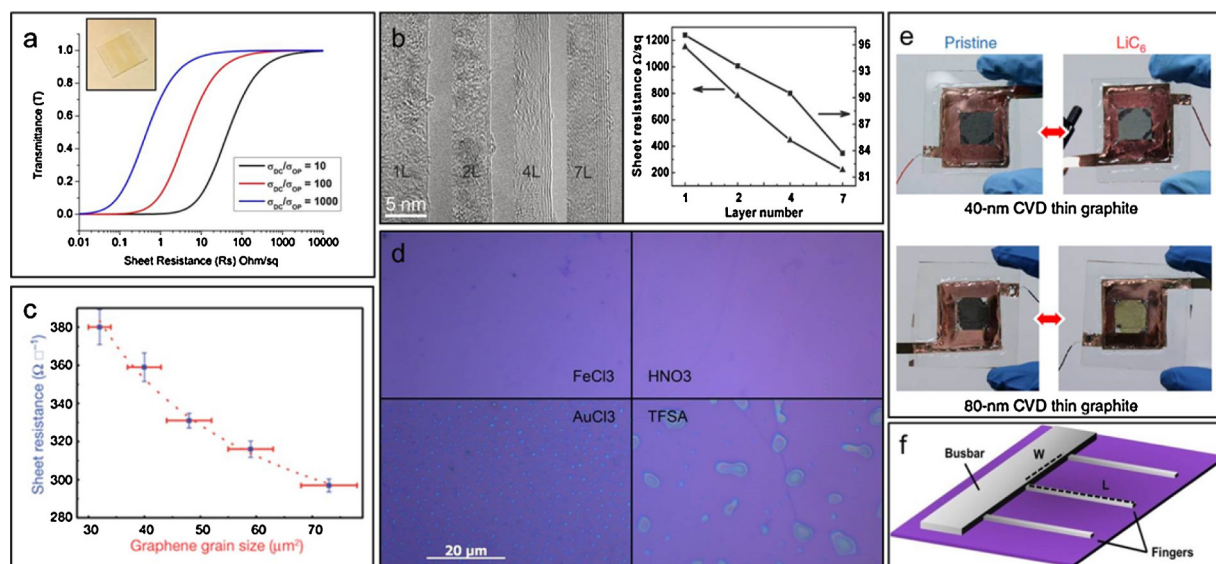


Figure 5 (a) Sheet resistance versus optical transmittance for various values of σ_{DC}/σ_{OP} . Inset: photograph of patterned ITO film on glass. (b) TEM images of few-layer graphene grown on copper foil via APCVD and sheet resistance and optical transmittance as a function of layer number. (c) Sheet resistance as a function of grain size. Dotted line is fitting curve. Reprinted with permission from [66]. Copyrights 2012 Nature Publishing Group. Reprinted with permission from [56]. Copyrights 2011 John Wiley and Sons. (d) Optical images of graphene after doping by various dopants. (e) Photographs of Li-intercalated CVD graphite and optical transmittance before and after intercalation. Reprinted with permission from [76]. Copyright 2014 Nature Publishing Group. (f) Illustration of hypothetical solar cell with finger length L and finger spacing W .

control because they are a function of the synthesis process, transfer process, substrate, encapsulating material, and any surface modifications. Thus, because synthesis/transfer processes can vary greatly between researchers, it is also difficult to compare values reported by different research groups. Therefore, any sheet resistance or mobility numbers cited in this section should be regarded as general trends rather than exact values.

Multilayer graphene (MLG) grown on nickel thin film typically has better sheet resistance than single-layer graphene (SLG) grown on copper but worse optical transmittance. With standard growth and transfer procedures, the sheet resistance of graphene samples typically ranges from 200–300 Ω/sq for multilayer graphene grown on Ni thin film and from 250 to 800 Ω/sq for monolayers grown on Cu. Some groups report values as low as 100 Ω/sq for Ni and 150 Ω/sq for copper [43,52]. Most researchers seem to prefer Cu-grown monolayer graphene because it usually has better σ_{DC}/σ_{OP} unless the mechanical robustness of multilayer films is required.

Stacking several monolayers can enhance the conductivity of the film at the expense of 2.3% optical transmittance per layer. However, the process of transferring multiple layers is time-consuming. Furthermore, in most cases, the sheet resistance does not decrease as $1/N$ (N is the number of layers) and the marginal benefit of each successive layer decreases as the number of layer increases [43,53–56]. This is likely because graphene is doped both by the substrate and from the atmosphere [57,58]. When there are multiple layers of graphene, the bottom layers are shielded from the atmosphere and the top layers are shielded from the substrate. Thus, each individual layer is less doped and has higher sheet resistance than an isolated monolayer.

Nonetheless, layer-by-layer stacking is one of the most popular methods of enhancing conductivity because it is easily applicable to actual devices. It is possible to directly synthesize few-layer graphene on copper directly, by using copper enclosures or atmospheric pressure CVD (APCVD) [56,59]. However, such techniques have had mixed results. Bi et al. controlled the number of layers by changing the hydrogen flow rate and growth time [56]. The SLG graphene films had sheet resistance of 1150 Ω/sq at 95.5% transmittance while the 7-layer films have sheet resistance of 220 Ω/sq at 82.2% transmittance (Fig. 5b). On the other hand, Li et al. showed that SLG synthesized via LPCVD has sheet resistance of 387 Ω/sq at 97.7% transmittance while APCVD-grown MLG has much higher sheet resistance of 500–1000 Ω/sq at 84–91% transmittance [60]. After transfer, thermal annealing is usually used to remove PMMA residue; this process also reduces the sheet resistance by increasing the intrinsic carrier concentration [61–66]. However, annealing requires heating the graphene to $>300^\circ\text{C}$, which is not possible for all types of devices. Duong et al. showed that increasing the graphene domain size by decreasing the methane concentration during growth can improve the sheet resistance from 400 to 300 Ω/sq (Fig. 5c). However, domain boundaries is only one of many sources of scattering in CVD graphene so the authors estimate that even with extremely large domains, the sheet resistance would saturate to 230 Ω/sq [66].

Chemical doping can be applied to further enhance the conductivity. Presently, the most commonly applied dopants are AuCl_3 and HNO_3 . Other dopants are MoO_3 , HCl , SOCl_2 , TFSA, (F4)TCNQ, and FeCl_3 . In all cases, dopant molecules are deposited onto graphene by spin-casting or evaporation. AuCl_3 , HNO_3 , TFSA, and FeCl_3 can reduce the

sheet resistance of graphene by 50–80% to 75–200 Ω/sq [43,67–71]. Using a combination of doping and layer stacking, researchers have achieved sheet resistances as low as 30 Ω/sq for 4-layer graphene, which is the lowest value for CVD graphene reported in literature thus far [43]. While this may seem promising, it is difficult to use doped graphene for some devices. HNO_3 , AuCl_3 , and FeCl_3 are all unstable in air so the doping effect gradually subsides over the course of several weeks [42,43,67]. AuCl_3 and TFSA leave significant particulate residue on the graphene surface, as shown in Fig. 5d, which is known to be detrimental for devices in which thin layers are deposited on top of the graphene [72,73]. All these dopants can also be removed by solvent rinsing, again making it difficult to fabricate structures on top of the graphene [70]. Because of these issues, many works that apply doped graphene use the graphene as the top electrode, which circumvents some of these issues.

Intercalation with FeCl_3 or Li may present viable routes to further enhance conductivity. Krapach et al. demonstrated a novel transparent conductor based on FeCl_3 -intercalated HOPG graphene with 8.8 Ω/sq at 84% transmittance [74]. The same intercalation technique was applied to epitaxial graphene grown on SiC to achieve 16 Ω/sq [75]. Unfortunately, it was found that FeCl_3 intercalation cannot be used for stacked layers of CVD graphene as the intercalation process appears to heavily damage the graphene [70]. Bao et al. showed that Li-intercalation can simultaneously enhance both the conductivity and optical transmittance of graphite [76]. The authors that 19-layer LiC_6 has sheet resistance of 3.0 Ω/sq at 91.7% transmittance, which corresponds to a $\sigma_{\text{DC}}/\sigma_{\text{OP}}$ value of 920 – exceeding that of ITO and actually breaking the theoretical limits of pristine graphene. This is explained by the fact that heavy n-doping suppresses optical transitions due to Pauli-blocking. The authors also demonstrated that their method can also be applied to thicker (40–80 nm) Ni-grown CVD graphene (Fig. 5e). While further work is necessary to scale up these techniques and to ensure that they are compatible with actual optoelectronic devices, these results suggest that further conductivity enhancements for CVD graphene may be possible.

Conductivity of liquid phase exfoliated graphene

Liquid phase exfoliated graphene is a network of interconnected few-layer flakes. The conductivity of the film is therefore a function of the physical properties of the individual flakes and the connectivity of the network. The perfect solution processed graphene film would consist of large monolayer flakes with no defects or impurities: multilayer flakes are less conductive, defects reduce the conductivity of individual flakes, impurities increase inter-flake resistance, and smaller flakes result in more inter-flake connections. In practice, solution-processed graphene films often have sheet resistances in the $\text{k}\Omega$ range, which is higher than that of CVD graphene. However, because liquid phase exfoliated graphene films typically consists of many layers, the conductivity is not as strongly influence by the substrate and environment. Like with CVD graphene, it is difficult to compare conductivity values between publications because of differences in fabrication methods and starting materials.

In general, graphene exfoliated in organic solvents or aqueous solutions with surfactant appear to perform worse

than electrochemically exfoliated graphene or rGO. This is likely because it is difficult to filter out the solvents and surfactants when depositing a film. Therefore, the impurities increase inter-flake resistance and reduces the conductivity of the film as a whole. Hernandez et al. found that films deposited after exfoliation in *N*-methyl-pyrrolidone (NMP) have up to 10 wt% in residual NMP even after drying and vacuum annealing [28]. Lotya et al. found that for aqueous graphene solutions, up to 36% of the weight of as-deposited films is residual surfactant, resulting in high sheet resistance of 970 $\text{k}\Omega/\text{sq}$ at 62% transmittance [29]. Furthermore, the process of violently sonicating graphite flakes breaks them up into much smaller flakes, which again reduces the film's conductivity. After an annealing step to remove the surfactant, the sheet resistance decreases to 22.5 $\text{k}\Omega/\text{sq}$, which corresponds to DC conductivity of 1500 S/m. These results suggest that annealing is essential, which limits the choice of substrate to those that can survive high temperatures.

With rGO, the oxidation process aids in separating individual layers and therefore harsh sonication is not required to exfoliate flakes. As a result, as demonstrated by Wang et al., flakes can be much larger, resulting in better quality films [77]. However, the process of actually reducing graphene oxide is non-trivial and the completeness of the reduction is critical to achieving good electrical performance. High temperature annealing (1100 °C in H_2) after hydrazine treatment is effective but again limits the choice of substrates to those that can survive such elevated temperatures [78]. Feng et al. showed that immersing in Na-NH_3 solution is also effective and can produce films with sheet resistance of 350 Ω/sq at 80% transmittance [79]. Electrochemical exfoliation, like rGO, can produce larger flakes and in addition, does not require a reduction step. Thus, films produced via this technique generally have reasonable sheet resistances and good C/O ratios without the need for high-temperature annealing [30].

Like with CVD graphene, chemical doping can also improve the conductivity of solution-processed films. We would expect that any dopant that works for CVD graphene should also work for solution-processed graphene. Parvez et al. showed that exposing films to HNO_3 for 2 h reduces their sheet resistance from 1.91 $\text{k}\Omega/\text{sq}$ to 330 Ω/sq at 80% transmittance, which is similar to that of nickel-grown CVD graphene [31]. At this point, it is unclear whether doped solution exfoliated graphene is more stable in air or in solvents than doped CVD graphene. Table 1 summarizes the above results.

Even though there is so much emphasis on matching the electrical performance of ITO, doing so may not be entirely necessary. For large-scale devices such as solar cells, TCs are used as charge collectors and short-range conductors while thicker metal busbars with fingers are used as long-range conductors. Assuming a simple busbar/finger geometry, as illustrated in Fig. 5f. (W is the finger spacing and L is the finger length), the average series resistance is $R_s \approx R_{\text{sh}}(W/4L)$, where R_{sh} is the sheet resistance of the TC. To determine the voltage drop caused by this series resistance, we multiply by the area and current density J_{SC} .

$$V_{\text{drop}} \sim R_{\text{sh}} \frac{W}{4L} \times (W \times L) \times J_{\text{SC}} = \frac{1}{4} R_{\text{sh}} W^2 J_{\text{SC}} \quad (3)$$

Table 1 Conductivity of liquid phase exfoliated graphene films.

Type	Flake thickness	Flake size	Other properties	Conductivity @ transmittance	Ref.
Disperse in organic solvents	—	<1 μm	—	5.1 k Ω /sq @ 42%	[28]
Disperse in water & surfactant	Mostly 1–2 Layer	<1 μm	—	22.5 k Ω /sq @ 62%	[29]
rGO	1.4 nm \pm 12%	364 nm \pm 33%	—	1000 Ω /sq @ 80%	[80]
rGO	—	20% >25 μm	—	760 S/m	[77]
rGO	—	—	2-step reduction	420 Ω /sq @ 61%	[78]
rGO (NaHN ₃)	—	—	16.6 C/O ratio	350 Ω /sq @ 80%	[79]
Electrochemical	80% 1–3 Layer	\sim 10 μm	12.3 C/O ratio	4.1 k Ω /sq @ 85%	[30]
Electrochemical	85% 1–3 Layer	80% >5 μm	HNO ₃ doped	2.4 k Ω /sq @ 73%	
				870 Ω /sq @ 91%	[31]
				330 Ω /sq @ 80%	

From this, we can see that if set V_{drop} to the maximum tolerable value (e.g. 50 mV), the maximum allowable finger spacing can be calculated as $W = \sqrt{(2V_{\text{drop}}/R_{\text{sh}}J_{\text{SC}})}$. Therefore, the finger spacing scales only as the inverse square root of sheet resistance i.e. if the sheet resistance of the TC increases by a factor of 4, the maximum allowable finger spacing decreases by only a factor of 2. If we look at the issue of scaling and conductivity from this viewpoint, we can see that we can compensate for the higher sheet resistance of graphene by reducing finger spacing. Thus, graphene may still be commercially viable if the cost reduction associated with using graphene instead of ITO can offset the performance penalty of reducing finger spacing. Despite these arguments, conductivity is still nonetheless the most important metric in many cases, especially for smaller area high-current devices such as LEDs. However, matching the performance of ITO should not be the sole determinant for whether or not graphene will be used in industry.

Optoelectronic devices with graphene electrodes

We now discuss the application of graphene as transparent electrodes in a variety of optoelectronic devices, illustrating the merits and drawbacks of using graphene as well as highlighting issues that still need to be addressed. Note that many works in literature use graphene for other purposes (such as the catalyst in DSSCs or the electron/hole transport layer (ETL/HTL) in organic solar cells and LEDs) but we focus on those that use graphene as transparent conductors.

Graphene/silicon Schottky barrier solar cells

Schottky barrier solar cells (SBSCs) – fabricated by placing a metal in contact with a semiconductor – are an alternative to conventional p–n solar cells. The metal induces band-bending in the semiconductor, resulting in a built-in electric field that can be used to collect photo-excited carrier. Silicon is the most common choice of semiconductor

but any semiconductor can be used provided that a metal with appropriate work function can be found. Maximizing Schottky barrier height is critical to achieving optical performance because larger barriers result in lower reverse saturation current and therefore higher V_{OC} . Thus, in general, high work function metals (gold) are used with p-type semiconductors and low-work function metals (aluminum) are used with n-type. This technology was widely investigated in the 1970s but has not been commercialized. Compared to conventional p–n bulk silicon solar cells, they are easier to fabricate and can potentially be used with lower-quality semiconductors because a high-temperature diffusion step is not required to form the p–n junction [81]. However, since metals are not transparent, conventional metal–silicon Schottky solar cells requires evaporating a metal grid with \sim 100 μm line spacing, which is an expensive and low-throughput process. Cheaper printed metal contacts, which are standard on p–n solar cells, are not suitable for SBSCs because the high temperature sintering process will introduce defects at the highly-sensitive metal–semiconductor interface [81].

Graphene-based SBSCs have been revisited in recent years because graphene offers several potential advantages to overcome the aforementioned limitations. First, graphene is optically transparent and can therefore be transferred over the entire active area without the need for patterning while coarse metal busbars/fingers can be used as long range conductors. This metallization strategy, combined with using cheaper, lower-quality silicon could make Schottky solar cells more competitive from a cost standpoint. Furthermore, the work function of graphene can be tuned by chemical doping or electrostatic gating to achieve the maximum Schottky barrier height.

Li et al. first demonstrated, in 2010, a proof-of-concept graphene/n-silicon SBSC with \sim 1.5% efficiency using a very simple fabrication procedure (Fig. 6a) [82]. The low efficiency was attributed to poor uniformity of the graphene sheets, poor interface quality, and mediocre optical transmittance. Several other efforts with very similar structures yielded very low efficiencies (<0.1%) due to low J_{SC} and poor fill factor [83–85]. This type of structure is one of

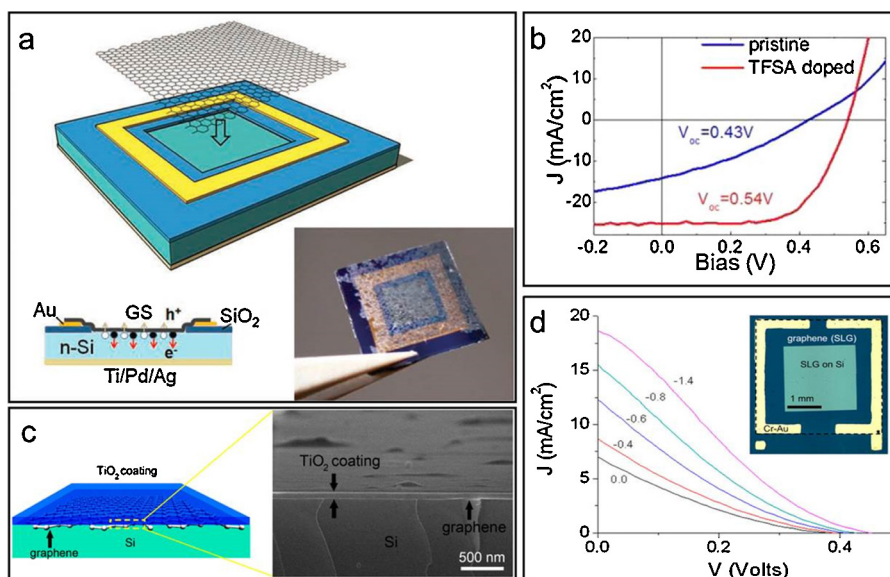


Figure 6 (a) The first graphene/n-silicon Schottky solar cell. All subsequent devices follow similar designs. Note that the Ni-grown graphene film is thick and non-uniform. Reprinted with permission from [82]. Copyright 2010 John Wiley and Sons. (b) Effect of p-doping (using TFSA) for such devices. Reprinted with permission from [86]. Copyright 2012 American Chemical Society. (c) Illustration and cross-sectional SEM image of colloidal TiO₂ anti-reflective coating. Reprinted with permission from [64]. Copyright 2013 American Chemical Society. (d) Effect of gating on graphene–silicon screen-engineered field-effect solar cells. Reprinted with permission from [92]. Copyright 2012 American Chemical Society.

the simplest optoelectronic devices that can be made using graphene TCs. The graphene is transferred on top of silicon, which can be immersed in water, so the standard PMMA-based transfer method works and residues are not too problematic. However, crystalline silicon outputs more current (up to 40 mA/cm²) than most thin-film technologies, making it critical to minimize the series resistance from the graphene. Efficiencies have increased drastically in recent years. In 2012, Miao et al. chemically doped the graphene using bis-(trifluoromethanesulfonyl)amide (TFSA) and achieved 8.6% efficiency (Fig. 6b) [86]. Other works were able to achieve similar efficiency values using other p-type dopants such as HNO₃ and SOCl₂ [60,87–90]. Chemical doping improves the efficiency of graphene/silicon solar cells in two ways. First, the increased carrier concentration greatly enhances the conductivity of the graphene film, thereby reducing series resistance and improving fill factor. In addition, hole-doping increases the work function of graphene, which raises the Schottky barrier height, thereby improving V_{oc}. The next large enhancement in PCE came in 2013, when Shi et al. applied a spin-on colloidal TiO₂ anti-reflective coating in conjunction with HNO₃ doping (Fig. 6c) [64]. The anti-reflective coating increased the J_{sc} to 32 mA/cm², resulting in a record 14.5% efficiency. An important point of this work is the combining of HNO₃ doping with the anti-reflective coating. The authors found that exposing their devices to HNO₃ vapor can still dope the graphene even after the anti-reflective coating is applied. This is likely because colloidal sol–gel TiO₂ is highly porous. Finally, we were able to further improve this figure to 15.6% by controlling the thickness of the native oxide between the graphene and silicon [91].

Novel graphene-on-silicon topologies have also been explored. Regan et al. demonstrated a screening-engineered field-effect solar cell using electrolyte-gated graphene [92]. Graphene was an appropriate choice for the electrode material because it is thin enough that it does not screen the electric field applied by the gate. In this case, the efficiency increased from 0.5% to 1.8% as gate voltage increased to –1.4 V, as shown in Fig. 6d. Lin et al. fabricated graphene/silicon solar cells on silicon nanopillars [89]. The silicon nanopillars were shown to form an effective anti-reflective coating – greatly increasing the J_{sc} – but the overall efficiency was only 7.7% as a result of the graphene film being discontinuous. We note that all works cited in this section use CVD graphene. To the best of the authors’ knowledge, graphene/n-silicon Schottky solar cells have not been demonstrated using solution processed graphene. Furthermore, metal–silicon Schottky solar cells are highly sensitive to the interface quality. We suspect that while a device with solution processed graphene can work in principle, these issues will severely hamper its performance. Furthermore, all current works on graphene–silicon devices use n-type silicon. This is a natural choice because graphene is intrinsically p-doped in air and can easily be p-doped further via chemical doping. However, n-doping techniques, such as Li-intercalation reported by Bao et al. will result in low-work function graphene and open the possibility of using p-type silicon [76].

A summary of efforts is shown in Table 2. Despite having achieved impressive efficiencies over a short period of time, the performance of graphene/silicon devices still lags behind that of conventional metal/silicon Schottky solar cells, which can be as high as 20% [93]. In fact, graphene

Table 2 Performance of graphene–silicon Schottky barrier solar cells.

Graphene	Dopant	J_{SC} [mA/cm ²]	V_{OC} [V]	FF [%]	PCE [%]	Notes	Ref.
ML Ni	–	6.5	0.48	56	1.7		[82]
SL Cu	–	14.2	0.43	32	1.9		[86]
	TFSA	25.3	0.54	63	8.6		
ML Cu	SOCl ₂	17.2	0.55	66	8.9	70 mW/cm ² illumination	[87]
	HNO ₃	17.1	0.55	69	9.3		
SL Cu	HNO ₃	19.4	0.56	54	8.3	70 mW/cm ² illumination	[60]
ML Cu	HNO ₃	16.9	0.55	73	9.6		
Not specified	HNO ₃	15.1	0.54	67	5.5		[88]
	SOCl ₂	17.9	0.55	61	6.0		
	H ₂ O ₂	16.9	0.55	55	5.1		
	HCl	16.8	0.55	53	4.9		
ML Pd	PCA/AuCl ₃	24.3	0.51	60	7.5		[90]
SL Cu	HNO ₃	32.0	0.62	72	14.5	With ARC	[64]
SL Cu	–				0.5–1.8	Gated	[92]
SL Cu	HNO ₃	22.7	0.52	66	7.7	Si Nanopillars	[89]
SL Cu	AuCl ₃	36.7	0.60	72	15.6	With ARC	[91]

devices are inferior in all performance metrics – V_{OC} , J_{SC} , and fill factor. Thus, further optimizations such as heavier graphene p-doping to enhance conductivity or better anti-reflective coatings are required to close the gap. It may also be worth exploring other options for performance enhancement such as textured silicon in conjunction with an anti-reflective coating for better light trapping. Most current reported devices have areas less than 1 cm² and it has been reported that performance decreases for larger device areas [64]. Thus, future investigations should be carried out regarding strategies for scaling up. Moreover, conventional Schottky solar cells suffer the crippling drawback of degrading in performance significantly over time due to the highly sensitive metal–silicon junction [81]. So far, no work has been done to determine whether graphene–silicon devices are stable for long-term use.

Organic solar cells

Organic solar cells are an emerging thin-film technology that offers the promise for very low-cost devices. They can be fabricated largely via solution processing and on a variety of cheap substrates such as plastic and paper, potentially allowing them to be mass-printed [94,95]. The best laboratory devices have shown efficiencies of nearly 10% for single-junction cells [96,97].

A recurrent theme in the works presented here is dealing with the hydrophobicity of the graphene film. For organic solar cell with ITO electrodes, standard fabrication procedure involves exposing the ITO to oxygen plasma to render it strongly hydrophilic and then spin-casting PEDOT:PSS as the hole transport layer (HTL), which is critical to the performance of the device. However, graphene is strongly hydrophobic and is etched by oxygen plasma, making it difficult to deposit this PEDOT:PSS layer. Furthermore, ITO devices with no HTL whatsoever still work (albeit with reduced V_{OC} and J_{SC}) [98] while graphene devices with a leaky HTL are essentially shorted [99]. This could be due to the rougher surface morphology of graphene or the

lower work function of graphene compared to ITO (~4.5 eV versus ~4.8 eV). Thus, it is critical that the HTL uniformly coats the graphene. Inverted devices (i.e. devices that use graphene as the cathode), which use zinc oxide as the electron transport layer (ETL) present similar issues. ZnO is most commonly deposited by dissolving zinc acetate in 2-methoxyethanol and spin-coating onto the electrode but 2-methoxyethanol does not wet graphene. In 2009, Wang et al. first demonstrated a P3HT:PCBM device with 1.7% PCE using nickel-grown CVD graphene as the anode [100]. The graphene was modified with pyrene buanoic acid succidymidyl ester to render the surface hydrophilic. Even after surface modification, the performance of these devices was considerably lower than that of their counterparts with ITO electrodes (3.1%). Yin et al. fabricated similar devices on PET using rGO as the bottom electrode [37]. Because the rGO films were thicker than CVD graphene films, they could be exposed to oxygen plasma for a short time. However, these devices only reached 0.8% efficiency, mostly due to the high sheet resistance of the rGO films. As the quality of graphene improved and researchers developed better ways to coat PEDOT:PSS onto hydrophobic surfaces, the gap between graphene devices and ITO devices soon closed. Park et al. found that AuCl₃ doping not only enhances the electrical conductivity of the graphene, but also makes the surface hydrophilic enough to spin-coat PEDOT:PSS [73]. Using these doped graphene electrodes, the authors were able to demonstrate 1.63% PCE for CuPc–C60 cells. AuCl₃ doping leaves gold particles up to 100 nm in height on the surface of the graphene, which was found to be undesirable for device performance. Similarly, Wang et al. evaporated thin layer of MoO_x onto graphene, making the surface hydrophilic and allowing them spin-coat PEDOT:PSS. This allowed them to achieve 2.5% efficiency for P3HT:PCBM devices – reasonably close to the 3.0% obtained using ITO [101].

Park et al. soon developed even more methods to circumvent the surface wettability issue. PEDOT:PSS can be deposited by alternative methods such as oxidative chemical vapor deposition (o-CVD) [102]. To apply this

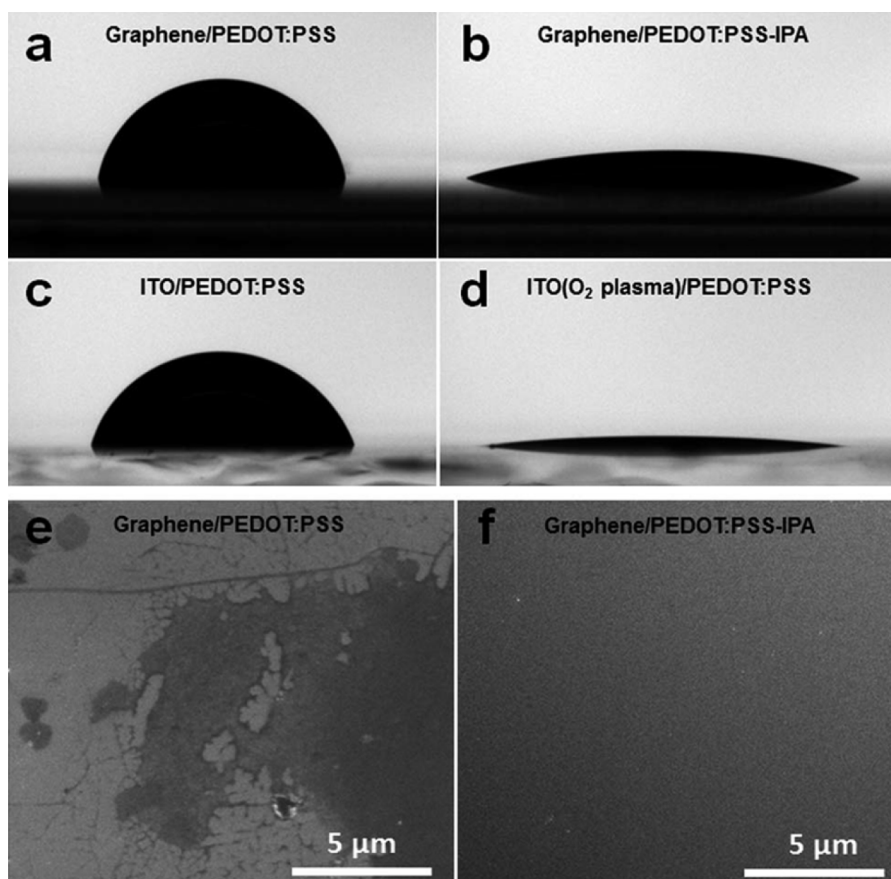


Figure 7 Droplets of (a) PEDOT:PSS and (b) PEDOT:PSS–IPA mixture on graphene; (b) PEDOT:PSS–IPA on graphene; PEDOT:PSS on (c) ITO after storage in air and on (d) ITO after O_2 plasma treatment; SEM images of (e) PEDOT:PSS on graphene and (f) PEDOT:PSS–IPA on graphene, showing the differences in coverage.

to organic devices, the authors co-evaporated the 3,4-ethylenedioxythiophene (EDOT) monomer along with $FeCl_3$ oxidant onto graphene, forming PEDOT films [103]. The PEDOT layer was uniform and devices fabricated on these films achieved 3.0% efficiency, compared to 3.2% for ITO reference devices. PEDOT:PSS can also be coated onto graphene by first coating a hydrophilic interlayer: PEDOT:PEG. By using PEDOT:PEG as an interfacial hole transport layer, Park et al. were able to achieve 2.9% for DBP/C60 cells with a graphene anode and 1.9% with graphene cathode compared to 3.1% and 2.1%, respectively for reference ITO devices [104]. A PEDOT:PEG interlayer also allows ZnO nanowires to be grown directly on graphene for PbS quantum dot devices, which achieved 4.9% efficiency [54]. Yin et al. also demonstrated inverted hybrid devices with rGO electrodes by electrochemically depositing ZnO nanorods on rGO [78]. Alternative hole transport layers are also possible. MoO_3 can be used as a substitute PEDOT:PSS for CuPc/C60 devices [105]. However, these devices exhibited very poor performance mostly owing to low V_{OC} and low fill factor. Another alternative hole transport material is poly(thiophene-3-[2-(2-methoxyethoxy)ethoxy]-2,5-diyl) (RG1200). RG-1200 is dissolved in ethylene glycol monobutyl ether, which allows it to be spin-coated directly onto graphene without any surface modification. Small molecule (DBP/C60/BCP) devices with graphene electrodes

and RG-1200 HTL had 2.72% PCE, which is nearly identical to that of reference ITO/RG-1200 devices (2.78%). Finally, mixing IPA with PEDOT:PSS 1:3 allows it to be uniformly coated onto graphene (Fig. 7) [99]. Using this solvent modified PEDOT:PSS, 50% of devices (DBP/C60) had performance similar to ITO reference devices while the other 50% had much poorer performance. However, adding a 20 nm layer of MoO_x on top of the IPA PEDOT improves the yield to 80%. Similar solvent-modification techniques can be applied to ETLs. Dissolving Zinc Acetate in methanol instead of 2-methoxy ethanol allows it to be uniformly spin-coated onto graphene [95], enabling Park et al. to fabricate inverted PTB7:PCBM solar cells on flexible substrates. This direction of research culminated in flexible PTB7:PCBM devices with efficiencies as high as 6.9%, which is currently the record for organic solar cells with graphene electrodes. Furthermore, these devices were shown to be stable even after 100 flexing cycles. Fig. 8 shows the progression in efficiency for OPVs with graphene electrodes.

The works references above all use graphene as the bottom electrode i.e. the organic layers were deposited on top of the graphene. There have also been efforts to apply graphene as the top electrode. As previously mentioned, an important point of concern in using graphene as the top electrode is that the typical graphene transfer process involves immersing the substrate in water but many organic

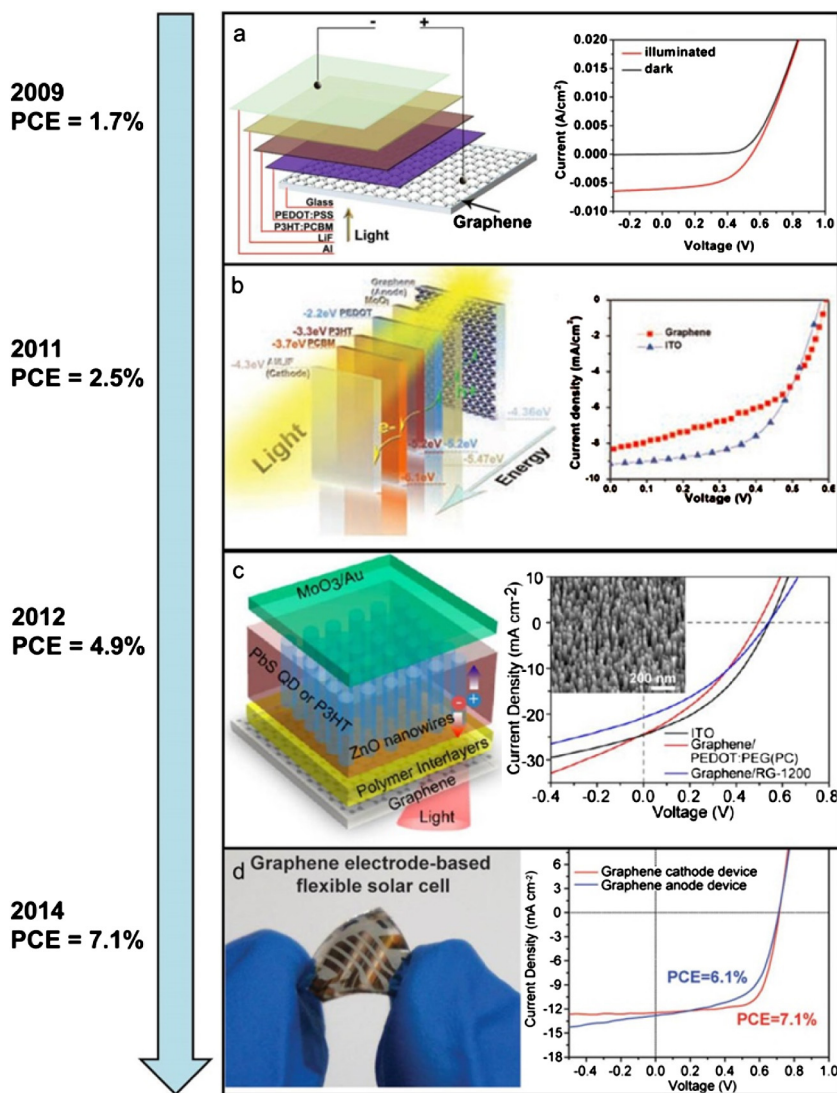


Figure 8 Device illustrations or photographs and corresponding *I/V* characteristics for: (a) P3HT:PCBM OPV with PBASE-modified graphene. Reprinted with permission from [100]. Copyright 2009 AIP Publishing. (b) P3HT:PCBM OPV with MoO_x interfacial layer. Reprinted with permission from [101]. Copyright 2011 John Wiley and Sons. (c) PbS QD hybrid device with ZnO nanowires grown on graphene. (d) PTB7:PCBM flexible devices with graphene anode and cathode.

layers are highly sensitive to oxygen and moisture [15]. In 2011, Lee et al. demonstrated a device compatible with roll-to-roll production by using a laminated graphene top electrode [106]. Graphene was transferred onto the device using thermal release tape as an intermediate transfer membrane, which does not require immersing in water. In 2012, Liu et al. achieved 2.7% efficiency for inverted P3HT:PCBM cells using ITO as the bottom electrode and single-layer graphene as the top electrodes [107]. These devices were semi-transparent and could be illuminated from either side though they consistently showed higher PCE when illuminated from the graphene side. The devices were baked in dry nitrogen after graphene transfer to remove residual moisture. In 2013, Liu et al. improved upon this device by using a metal bottom electrode instead of ITO (Fig. 9a), as the transparent graphene top electrode obviates the need for a transparent bottom electrode. Furthermore, they showed two or more layers of graphene as the top electrode

effectively encapsulates the devices and minimizes degradation over time (Fig. 9b) [108]. Tong et al. demonstrated a novel proof-of-concept device topology using graphene as the intermediate layer between two series or parallel tandem devices (Fig. 9c) [109]. In this work, the series configuration had PCE lower than that of the bottom sub-cell but the parallel configuration was able to achieve 2.9% PCE, which was 88% of the sum of the PCEs of the two sub-cells. The nickel-grown graphene was transferred using a PDMS stamp.

It is clear that graphene is effective as a transparent electrode material for both small molecule and bulk heterojunction organic solar cells. However, extra fabrication steps or non-standard graphene transfer techniques are necessary to ensure that the graphene electrode is compatible. In most cases, the performance of devices with graphene electrodes is similar to, but still slightly lower than, that of reference ITO devices. Since the works referenced above

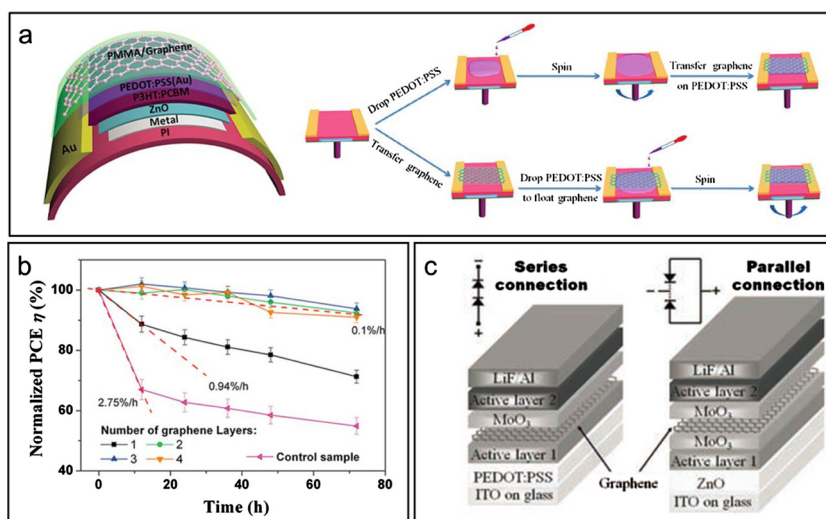


Figure 9 (a) Device structure and graphene transfer procedure for organic solar cell using graphene top electrode. (b) Stability in air as a function of the number of graphene layers. (a) and (b) reprinted with permission from [107,108]. Copyright 2012 American Chemical Society, 2013 John Wiley and Sons. (c) Series and parallel connections for device with graphene intermediate electrode. Reprinted with permission from [109]. Copyright 2011 John Wiley and Sons.

Table 3 Performance of organic solar cells using graphene electrodes.

Active material	Graphene type	Topology	PCE [%]	ITO Ref. [%]	Ref.
P3HT/PCBM	Single-layer Ni	Top/cathode	2.7%	3.1%	[107,108]
P3HT/PCBM	MLNi	Middle	2.9%	—	[109]
P3HT/PCBM	Stacked Cu	Bottom/cathode	2.3	3.1	[104]
P3HT/PCBM	rGO	Bottom/anode	0.78	—	[37]
P3HT/PCBM	rGO	Bottom/cathode	0.38	—	[78]
CuPc/C60	ML Ni	Bottom/anode	1.63	1.77	[73]
DBP/C60	Stacked Cu	Bottom/anode	2.7–3.0	2.8–3.2	[99,103,104,110]
DBP/C60	Stacked Cu	Bottom/cathode	1.9	2.1	[104]
PbS QD	Stacked Cu	Bottom/cathode	4.2	5.1	[54]
PTB7/PCBM	Stacked Cu	Bottom/(anode and cathode)	6.1–7.1	6.7–7.6	[95]

only deal with millimeter-to-centimeter-scale devices, in the future, it will be necessary to demonstrate larger-scale devices to prove that graphene electrodes are reliable and scalable. It is also worth noting that organic solar cells themselves have not yet been commercialized. This represents an interesting opportunity, as the electrode material can be developed in parallel with the active material. Thus, there may be less resistance to adopting graphene as the standard TC for organic solar cells than for other, more established, technologies. A summary of efforts can be found in Table 3.

Other solar cells

Dye sensitized solar cells (DSSCs) is an emerging photovoltaic technology. The fabrication process for DSSCs involves sintering titania paste or platinum paste at $>400^{\circ}\text{C}$. As a result, fluorine-doped tin oxide (FTO) is preferred over ITO for the TC because it has better thermal stability even though it has worse conductivity. Therefore, graphene, which also has good thermal stability, may be a suitable alternative. To date, there are many reports of graphene used in DSSCs

but very few of these use graphene as the TC. In 2008, Wang et al. first used rGO as the anode for DSSCs [111]. Because both graphene and DSSC technology was still in its infancy at the time, the resulting efficiency was only 0.26% compared to 0.84% for FTO reference devices. In 2011, Bi et al. demonstrated DSSCs with 4.25% efficiency using CVD graphene as the counter electrode [112]. This work was quite unique in that the graphene used was synthesized directly on SiO_2 rather than on a metal foil. Dong et al. applied a novel graphene vertically-aligned nanotube hybrid network as the counter-electrode [113]. Here, the graphene/CNT network was synthesized on nickel foil and the Ni/graphene/CNT stack was then directly used as the flexible counter-electrode. The PCE was 8.2% for rigid devices and 3.9% for flexible devices.

GaAs is a high-efficiency thin-film technology – with PCEs as high as 28.8% for single-junction devices [114]. However, the expensive fabrication process restricts its usage to applications such as satellites, where performance is more important than cost. Recently, researchers have begun investigating graphene/GaAs SBSCs. In terms of operating

principle, these devices are very similar to graphene/silicon solar cells but can achieve higher V_{OC} values because GaAs has a higher bandgap of 1.4 eV. Like with graphene/silicon devices, efficiencies were initially low and improved over time [115]. Li et al. achieved 18.5% PCE by chemically doping the graphene, applying an anti-reflective coating, and electrostatically gating the device with a top gate [116]. Since GaAs is intrinsically a high-efficiency technology, we expect this figure to improve with further optimizations. However, like with graphene/silicon devices, more work is necessary to demonstrate concrete advantages of graphene over metal grids.

CdTe is the industry dominant thin-film technology, boasting PCE values of nearly 20% for laboratory devices. Like organic solar cells, these devices can be fabricated on flexible substrates such as Kapton[®], which encouraged researchers to investigate alternative TCs. Lin et al. developed a novel synthesis procedure to produce boron-doped graphene flakes and used this as the back electrode for a CdTe solar cell [117]. Devices made with boron-doped graphene reached 7.86% efficiency, outperforming devices made with pristine graphene or rGO. Bi et al. demonstrated a CdTe solar cell using CVD graphene as the front electrode [56]. These devices showed excellent J_{SC} of 22.9 mA/cm² but were limited by poor V_{OC} and FF, resulting in overall efficiency of 4.17%. The former work used graphene as the back electrode (i.e. the graphene was deposited last) while the latter used graphene as the front electrode (i.e. subsequent layers were deposited onto the graphene). Despite how promising the technology may be, at the moment, there does not appear to be many groups pursuing CdTe devices with graphene electrodes. This is possibly because of the toxicity of the materials or because CdTe solar cells are already prevalent in industry with ITO electrodes and therefore do not require further modifications.

Other thin-film solar cell technologies include amorphous silicon (a-Si) and more recently, perovskite. Amorphous silicon is also a very low-cost technology. In 2010, Schriver et al. used graphene as the top electrode for a-Si devices. However, open-circuit voltage was only 150 mV for graphene devices and PCE was very low. Since then, there have not been any subsequent works on the subject, which may possibly be because other thin-film technologies such as CdTe show better performance. Perovskite solar cells is relatively new technology that combines the low-cost of organic solar cells with very high efficiencies (approaching 20%) compared to other thin-film technologies [118,119]. Recently, You et al. demonstrated semitransparent perovskite solar cell with PCE as high as 12% using graphene as the top electrode [120]. This represents the highest efficiency for thin-film solar cells with graphene electrodes thus far. Like organic solar cells, many of these thin-film technologies have not been commercialized, which presents opportunities for graphene if some synergy (e.g. cost, flexibility, temperature resistance) can be found between the graphene and the active layer.

Light emitting diodes

Because LEDs typically carry higher current densities than solar cells, the conductivity requirement is higher for

graphene electrodes. Solar cells typically operate at less than 1 V and have current densities of about 20–40 mA/cm² for silicon devices and 3–20 mA/cm² for organic devices whereas LEDs can operate at 5–10 V and maximum current is limited by the thermal properties of the device.

There are two main classes of LEDs – organic (OLEDs) and inorganic. Unlike organic solar cells, which have yet to be commercialized, OLEDs are commonly used in digital displays such as televisions and computer screens. In 2010, Wu et al. first demonstrated OLEDs using rGO as the anode (Fig. 10a) [121]. The rGO had sheet resistance of 800 Ω /sq with optical transmittance of 82%, which is much worse than the 20 Ω /sq of reference commercial ITO films. As a result, the graphene devices had significantly lower external quantum efficiency and luminous power efficiency than ITO reference devices. Sun et al. constructed similar devices using multilayer CVD graphene with sheet resistance of 310 Ω /sq at 85% transmittance [122]. The maximum power efficiency was 0.38 lm/W at 5.8 V, which is similar to that reported for the aforementioned devices with rGO electrodes. The authors state that performance was not as good

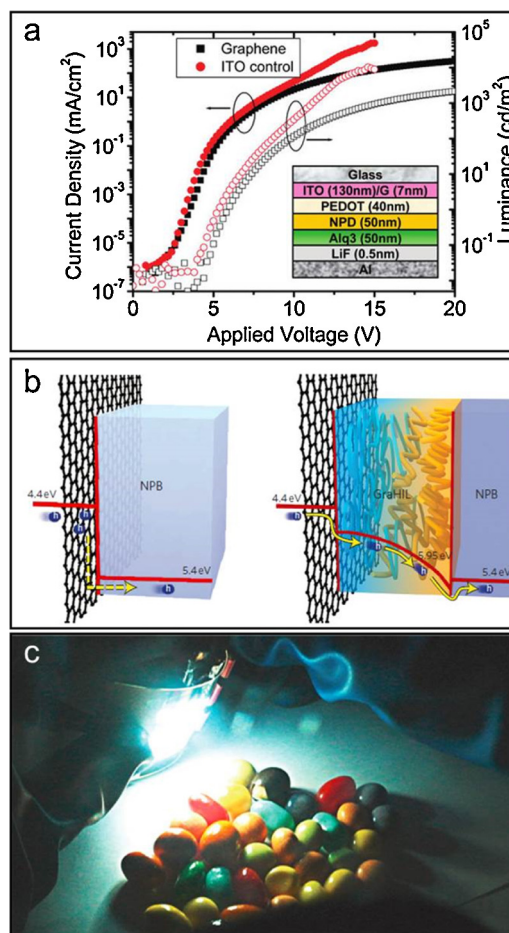


Figure 10 (a) Structure and performance of OLED with rGO electrodes compared to ITO references. Reprinted with permission from [121]. Copyright 2010 American Chemical Society. (b) Comparison of standard structure to the gradual hole injection layer developed by Han et al. and (c) photograph of white LEDs with graphene electrodes. (b and c) Reprinted with permission from [72]. Copyright 2012 Nature Publishing Group.

as typical values reported for ITO-based devices, with surface roughness and high sheet resistance of the multi-layer graphene film cited as possible reasons.

Like with graphene-based organic solar cells, efficiencies steadily improved over time. In 2012, Han et al. demonstrate, for the first time, graphene devices with performance superior to that of ITO references [72]. The authors believed that part of the reason for poor performance in the past is that the work function of graphene is lower than that of ITO. As a result, there is a large barrier between the graphene and the organic layers, resulting in high contact resistance, which hampers hole injection from the graphene. To address this issue, the authors used a gradual hole injection layer (Fig. 10b) as well as chemically doping the graphene to raise its work function; 4-layer graphene was doped with HNO_3 or AuCl_3 , resulting in sheet resistance of $54 \Omega/\text{sq}$ and $34 \Omega/\text{sq}$, respectively. The exceptionally low sheet resistances obtained in this work contributed to the performance (Fig. 10c). The power efficiency was 37.2 lm/W for fluorescent devices and 102.7 lm/W for phosphorescent devices, which represents a 100-fold improvement over past works. Thus, it would

appear that doping graphene to lower the sheet resistance and developing techniques for optimizing contact resistance are critical to high-performance OLED devices. Li et al. and Meyer et al. achieved similarly impressive results using triethyloxonium hexachloroantimonate doped single-layer graphene and MoO_x -doped few layer graphene electrodes, respectively [123,124]. More work is necessary to determine whether these devices can be scaled up and fabricated with high enough yield for digital displays. Unlike many of the other technologies discussed here, OLEDs are a relatively mature field and is now widely-used in electronic displays. Thus, there is a constant push toward cheaper, more reliable devices, which presents opportunities for graphene if enough advantages can be found.

Because graphene offers good transmittance in the UV and near-IR regimes, some efforts have also been made to incorporate graphene electrodes into inorganic UV LEDs. Similar to the case of organic/inorganic solar cells, these works primarily focus on using graphene as the top electrode. Again, like inorganic solar cells, chemical doping is necessary to improve the conductivity of the graphene and enhance device performance. Kim et al.

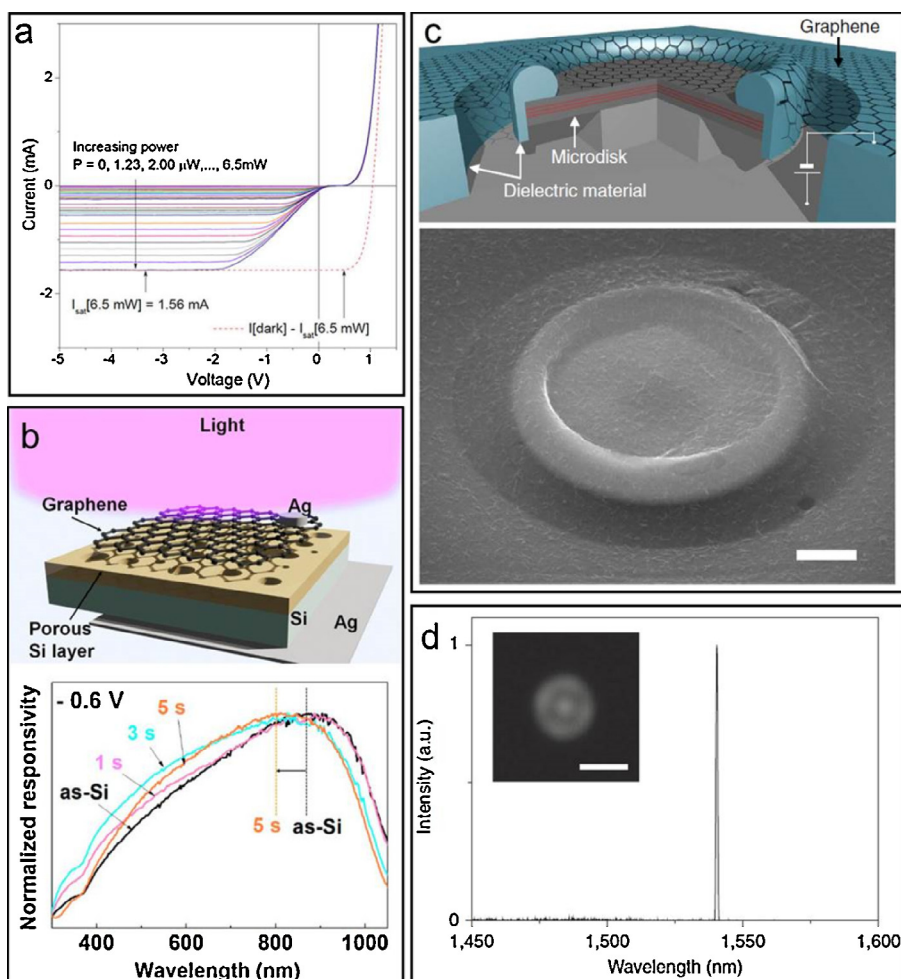


Figure 11 (a) J/V characteristics as a function of illumination intensity for graphene–silicon photodetectors. Reprinted with permission from [127]. Copyright 2013 American Chemical Society. (b) Schematic of graphene–porous silicon photodetectors and plot showing the superior responsivity at near-UV wavelengths. Reprinted with permission from [128]. Copyright 2014 American Chemical Society. (c) Illustration and SEM image of electrically driven microdisk lasers with graphene top contact and (d) output spectrum. Reprinted with permission from [129]. Copyright 2012 Nature Publishing Group.

applied AuCl₃-doped graphene as the top electrode for GaN-based ultraviolet (UV) LEDs [125]. It was determined that doping using 10 mM AuCl₃ is optimal due to the trade-off between sheet resistance and optical transmittance. Youn et al. used HNO₃-doped graphene as the top electrode for GaN LEDs [126]. Because graphene does not make a good ohmic contact with p-type GaN, the authors used Cr/Au to make a point contact with the GaN and doped graphene as the long-range conductor.

Other devices

Other applications for graphene electrodes include touch panels, photodetectors, and semiconductor lasers. Touch panels are ubiquitous in modern electronics. Graphene may be a suitable TC for these devices because they use very little current, which means the conductivity requirement is more lax. Bae et al. applied their roll-to-roll transfer method to create graphene-based resistive touch screens [43]. Two graphene/PET films are sandwiched together with spacers in between and the two graphene layers make contact when pressure is applied. Because there has been a recent technological trend toward flexible displays, graphene may be promising for this direction of research. An et al. showed that graphene transferred onto silicon can be used as a tunable high-sensitivity photodetector (Fig. 11a) [127]. Here, the silicon is responsible for collecting light and generating electron–hole pairs while the graphene is responsible for collecting these carriers. These devices showed excellent responsivity of 435 mA/W and response times in the millisecond range. Furthermore, the unique band structure of graphene allows the photocurrent to be easily tuned by applying a reverse bias with ON/OFF ratios as high as 10⁴. Recently, Kim et al. fabricated similar devices on porous silicon (Fig. 11b) [128]. The porous silicon devices showed significantly improved quantum efficiency in the near-ultraviolet regime compared to devices with flat silicon. It is worth noting that in both these works, the devices require some reverse bias to achieve the best responsivity but the leakage current due to the reverse bias is minimal. Kim et al. used CVD graphene grown on nickel thin film as a transparent conductor for electrically-driven microdisk lasers (Fig. 11c and d) [129]. One major challenge in building nanophotonic devices is that placing an electrical conductor near the device can interfere with its optical properties. However, because graphene is so thin, it provides a robust current path without influencing the optical cavity. Thus, this work truly leverages the atomic thinness of the graphene and may pave the path for further work in the field. However, contact resistance between graphene and metals tends to quite high – commonly in the range of 250–2000 Ω μm – which may hamper small-scale devices such as these lasers or photodetectors [130,131]. Thus, further research is needed to reduce graphene–metal contact resistances in order to improve the performance of larger arrays of graphene-based devices.

Conclusion

Remarkable progress in understanding and applying graphene has been made over the last decade. Many

different applications of graphene have been explored and transparent electrode for optoelectronics is an important one among them. Researchers have demonstrated working solar cells, LEDs, photodetectors, and lasers using graphene electrodes. Though the anticipated advantages of using graphene has been verified, at this stage graphene-based technology has not demonstrated enough benefits in performance, reproducibility and stability, cost, and various other considerations to warrant replacing ITO in industry. In addition, the scaling up of graphene production (either CVD or liquid phase exfoliation) and transfer still needs further development. Maturation of graphene-based applications will certainly boost these manufacturing and processing technologies, which in turn will open up the possibility for more applications.

Comparing to other emerging TC technologies like metal nanowires, CNTs, and conductive polymers, research in graphene has advanced quickly. Although investigations in these other material systems started much earlier, at present CNT-based TCs are the only one among them that has begun to reach commercialization in touch screen products. It is anticipated that graphene will catch up soon. Furthermore, combining graphene with other technologies to capture the advantages of both has also yielded even more promising results. For example, graphene–metal nanowire hybrid films are shown to be remarkably stretchable and are much more conductive than graphene alone [132]. And a recent roll-to-roll technology incorporating both metal nanowires (or nano trough) together with graphene transferred onto flexible substrates has demonstrated superior transparency/sheet resistance ratio, reduced surface roughness and offered better stability in air due to the fact that the nanowires were encapsulated by the polymer substrate and graphene [133]. Researchers have also demonstrated the synthesis of seamless graphene–CNT hybrid networks, which are being applied to DSSCs [113,134]. These hybrid technologies also present exciting opportunities for future research.

Overall, graphene is still a relatively young material. The study of carbon nanotubes began in 1991 but only recently have companies begun exploring nanotube films for large-scale optoelectronic devices [135,136]. If we use the time between synthesis and commercialization for CNTs as the metric, we might expect graphene-based optoelectronic devices to be industrially produced in the next one to two decade. However, this could happen much sooner since research in the field is now driven by faster information propagation and increasing demand for electronics. Although there are still many challenges that must be overcome, each challenge also presents a prospect for further research. Given the remarkable rate of progress so far, we are optimistic that researchers can continue developing new technologies to address these challenges in the near future.

Acknowledgements

The authors gratefully acknowledge financial support for this work from Eni S.p.A. under the Eni-MIT Alliance Solar Frontiers Center.

References

- [1] L.B. Hu, H. Wu, Y. Cui, *Mater. Res. Soc. Bull.* 36 (2011) 760–765.
- [2] C.F. Guo, Z.F. Ren, *Mater. Today* 18 (2015) 143–154.
- [3] D.S. Hecht, L.B. Hu, G. Irvin, *Adv. Mater.* 23 (2011) 1482–1513.
- [4] S. Park, M. Vosguerichian, Z.A. Bao, *Nanoscale* 5 (2013) 1727–1752.
- [5] J.H. Du, S.F. Pei, L.P. Ma, H.M. Cheng, *Adv. Mater.* 26 (2014) 1958–1991.
- [6] D.J. Lipomi, J.A. Lee, M. Vosguerichian, B.C.K. Tee, J.A. Bolander, Z.A. Bao, *Chem. Mater.* 24 (2012) 373–382.
- [7] A. Elschner, W. Lovenich, *Mater. Res. Soc. Bull.* 36 (2011) 794–798.
- [8] J.H. Chen, C. Jang, S.D. Xiao, M. Ishigami, M.S. Fuhrer, *Nat. Nanotechnol.* 3 (2008) 206–209.
- [9] R.R. Nair, P. Blake, A.N. Grigorenko, K.S. Novoselov, T.J. Booth, T. Stauber, N.M.R. Peres, A.K. Geim, *Science* 320 (2008) 1308.
- [10] C.H. Lee, M.K. Jeong, M.F. Kılıcaslan, J.H. Lee, H.S. Hong, S.J. Hong, *Waste Manage.* 33 (2013) 730–734.
- [11] M. Girtan, M. Rusu, *Sol. Energy Mater. Sol. Cells* 94 (2010) 446–450.
- [12] M. Jorgensen, K. Norrman, F.C. Krebs, *Sol. Energy Mater. Sol. Cells* 92 (2008) 686–714.
- [13] K.S. Novoselov, A.K. Geim, S.V. Morozov, D. Jiang, Y. Zhang, S.V. Dubonos, I.V. Grigorieva, A.A. Firsov, *Science* 306 (2004) 666–669.
- [14] X.S. Li, W.W. Cai, J.H. An, S. Kim, J. Nah, D.X. Yang, R. Piner, A. Velamakanni, I. Jung, E. Tutuc, S.K. Banerjee, L. Colombo, R.S. Ruoff, *Science* 324 (2009) 1312–1314.
- [15] A. Reina, X.T. Jia, J. Ho, D. Nezich, H.B. Son, V. Bulovic, M.S. Dresselhaus, J. Kong, *Nano Lett.* 9 (2009) 30–35.
- [16] G.D. Ruan, Z.Z. Sun, Z.W. Peng, J.M. Tour, *ACS Nano* 5 (2011) 7601–7607.
- [17] Z.Z. Sun, Z. Yan, J. Yao, E. Beitler, Y. Zhu, J.M. Tour, *Nature* 468 (2010) 549–552.
- [18] C.C. Wang, W. Chen, C. Han, G. Wang, B.B. Tang, C.X. Tang, Y. Wang, W.N. Zou, W. Chen, X.A. Zhang, S.Q. Qin, S.L. Chang, L. Wang, *Sci. Rep. (UK)* 4 (2014), 4537.
- [19] Y.F. Hao, M.S. Bharathi, L. Wang, Y.Y. Liu, H. Chen, S. Nie, X.H. Wang, H. Chou, C. Tan, B. Fallahzad, H. Ramanarayan, C.W. Magnuson, E. Tutuc, B.I. Yakobson, K.F. McCarty, Y.W. Zhang, P. Kim, J. Hone, L. Colombo, R.S. Ruoff, *Science* 342 (2013) 720–723.
- [20] A. Mohsin, L. Liu, P.Z. Liu, W. Deng, I.N. Ivanov, G.L. Li, O.E. Dyck, G. Duscher, J.R. Dunlap, K. Xiao, G. Gu, *ACS Nano* 7 (2013) 8924–8931.
- [21] K.V. Emtsev, A. Bostwick, K. Horn, J. Jobst, G.L. Kellogg, L. Ley, J.L. McChesney, T. Ohta, S.A. Reshanov, J. Rohrl, E. Rotenberg, A.K. Schmid, D. Waldmann, H.B. Weber, T. Seyller, *Nat. Mater.* 8 (2009) 203–207.
- [22] J.H. Lee, E.K. Lee, W.J. Joo, Y. Jang, B.S. Kim, J.Y. Lim, S.H. Choi, S.J. Ahn, J.R. Ahn, M.H. Park, C.W. Yang, B.L. Choi, S.W. Hwang, D. Whang, *Science* 344 (2014) 286–289.
- [23] T. Hesjedal, *Appl. Phys. Lett.* 98 (2011), 133106.
- [24] T. Yamada, M. Ishihara, J. Kim, M. Hasegawa, S. Iijima, *Carbon* 50 (2012) 2615–2619.
- [25] T. Kobayashi, M. Bando, N. Kimura, K. Shimizu, K. Kadono, N. Umezū, K. Miyahara, S. Hayazaki, S. Nagai, Y. Mizuguchi, Y. Murakami, D. Hobar, *Appl. Phys. Lett.* 102 (2013), 023112.
- [26] J. Hofrichter, B.N. Szafraneck, M. Otto, T.J. Echtermeyer, M. Baus, A. Majerus, V. Geringer, M. Ramsteiner, H. Kurz, *Nano Lett.* 10 (2010) 36–42.
- [27] D.Q. McNerny, B. Viswanath, D. Copic, F.R. Laye, C. Prohoda, A.C. Brieland-Shoultz, E.S. Polsen, N.T. Dee, V.S. Veerasamy, A.J. Hart, *Sci. Rep. (UK)* 4 (2014), 5049.
- [28] Y. Hernandez, V. Nicolosi, M. Lotya, F.M. Blighe, Z. Sun, S. De, I.T. McGovern, B. Holland, M. Byrne, Y.K. Gun'ko, J.J. Boland, P. Niraj, G. Duesberg, S. Krishnamurthy, R. Goodhue, J. Hutchison, V. Scardaci, A.C. Ferrari, J.N. Coleman, *Nat. Nano* 3 (2008) 563–568.
- [29] M. Lotya, Y. Hernandez, P.J. King, R.J. Smith, V. Nicolosi, L.S. Karlsson, F.M. Blighe, S. De, Z. Wang, I.T. McGovern, G.S. Duesberg, J.N. Coleman, *J. Am. Chem. Soc.* 131 (2009) 3611–3620.
- [30] K. Parvez, R. Li, S.R. Puniredd, Y. Hernandez, F. Hinkel, S. Wang, X. Feng, K. Müllen, *ACS Nano* 7 (2013) 3598–3606.
- [31] K. Parvez, Z.-S. Wu, R. Li, X. Liu, R. Graf, X. Feng, K. Müllen, *J. Am. Chem. Soc.* 136 (2014) 6083–6091.
- [32] L.J. Cote, R. Cruz-Silva, J. Huang, *J. Am. Chem. Soc.* 131 (2009) 11027–11032.
- [33] C. Gómez-Navarro, R.T. Weitz, A.M. Bittner, M. Scolari, A. Mews, M. Burghard, K. Kern, *Nano Lett.* 7 (2007) 3499–3503.
- [34] M. Zhou, J. Tang, Q. Cheng, G. Xu, P. Cui, L.-C. Qin, *Chem. Phys. Lett.* 572 (2013) 61–65.
- [35] W.S. Hummers, R.E. Offeman, *J. Am. Chem. Soc.* 80 (1958) 1339.
- [36] H.Y. He, J. Klinowski, M. Forster, A. Lerf, *Chem. Phys. Lett.* 287 (1998) 53–56.
- [37] Z.Y. Yin, S.Y. Sun, T. Salim, S.X. Wu, X.A. Huang, Q.Y. He, Y.M. Lam, H. Zhang, *ACS Nano* 4 (2010) 5263–5268.
- [38] G.B. Barin, Y. Song, I.D. Gimenez, A.G. Souza, L.S. Barretto, J. Kong, *Carbon* 84 (2015) 82–90.
- [39] X.S. Li, Y.W. Zhu, W.W. Cai, M. Borysiak, B.Y. Han, D. Chen, R.D. Piner, L. Colombo, R.S. Ruoff, *Nano Lett.* 9 (2009) 4359–4363.
- [40] X.L. Liang, B.A. Sperling, I. Calizo, G.J. Cheng, C.A. Hacker, Q. Zhang, Y. Obeng, K. Yan, H.L. Peng, Q.L. Li, X.X. Zhu, H. Yuan, A.R.H. Walker, Z.F. Liu, L.M. Peng, C.A. Richter, *ACS Nano* 5 (2011) 9144–9153.
- [41] K.S. Kim, Y. Zhao, H. Jang, S.Y. Lee, J.M. Kim, K.S. Kim, J.H. Ahn, P. Kim, J.Y. Choi, B.H. Hong, *Nature* 457 (2009) 706–710.
- [42] J. Song, F.Y. Kam, R.Q. Png, W.L. Seah, J.M. Zhuo, G.K. Lim, P.K.H. Ho, L.L. Chua, *Nat. Nanotechnol.* 8 (2013) 356–362.
- [43] S. Bae, H. Kim, Y. Lee, X.F. Xu, J.S. Park, Y. Zheng, J. Balakrishnan, T. Lei, H.R. Kim, Y.I. Song, Y.J. Kim, K.S. Kim, B. Ozyilmaz, J.H. Ahn, B.H. Hong, S. Iijima, *Nat. Nanotechnol.* 5 (2010) 574–578.
- [44] L.G.P. Martins, Y. Song, T.Y. Zeng, M.S. Dresselhaus, J. Kong, P.T. Araujo, *Proc. Natl. Acad. Sci. U.S.A.* 110 (2013) 17762–17767.
- [45] G.H. Han, H.J. Shin, E.S. Kim, S.J. Chae, J.Y. Choi, Y.H. Lee, *Nano* 6 (2011) 59–65.
- [46] S.C. O'Hern, C.A. Stewart, M.S.H. Boutilier, J.C. Idrobo, S. Bhaviripudi, S.K. Das, J. Kong, T. Laoui, M. Atieh, R. Karnik, *ACS Nano* 6 (2012) 10130–10138.
- [47] Y. Wang, Y. Zheng, X.F. Xu, E. Dubuisson, Q.L. Bao, J. Lu, K.P. Loh, *ACS Nano* 5 (2011) 9927–9933.
- [48] E.H. Lock, M. Baraket, M. Laskoski, S.P. Mulvaney, W.K. Lee, P.E. Sheehan, D.R. Hines, J.T. Robinson, J. Tosado, M.S. Fuhrer, S.C. Hernandez, S.G. Waltont, *Nano Lett.* 12 (2012) 102–107.
- [49] L.B. Gao, W.C. Ren, H.L. Xu, L. Jin, Z.X. Wang, T. Ma, L.P. Ma, Z.Y. Zhang, Q. Fu, L.M. Peng, X.H. Bao, H.M. Cheng, *Nat. Commun.* 3 (2012), 699.
- [50] K.I. Bolotin, K.J. Sikes, Z. Jiang, M. Klima, G. Fudenberg, J. Hone, P. Kim, H.L. Stormer, *Solid State Commun.* 146 (2008) 351–355.
- [51] M.W. Rowell, M.D. McGehee, *Energy Environ. Sci.* 4 (2011) 131–134.
- [52] Y.P. Gong, X.M. Zhang, G.T. Liu, L.Q. Wu, X.M. Geng, M.S. Long, X.H. Cao, Y.F. Guo, W.W. Li, J.B. Xu, M.T. Sun, L. Lu, L.W. Liu, *Adv. Funct. Mater.* 22 (2012) 3153–3159.

- [53] S. Lee, K. Lee, C.H. Liu, Z.H. Zhong, *Nanoscale* 4 (2012) 639–644.
- [54] H. Park, S. Chang, J. Jean, J.J. Cheng, P.T. Araujo, M.S. Wang, M.G. Bawendi, M.S. Dresselhaus, V. Bulovic, J. Kong, S. Gradečak, *Nano Lett.* 13 (2013) 233–239.
- [55] T.H. Yu, C.W. Liang, C. Kim, E.S. Song, B. Yu, *IEEE Electr. Device Lett.* 32 (2011) 1110–1112.
- [56] H. Bi, F.Q. Huang, J. Liang, X.M. Xie, M.H. Jiang, *Adv. Mater.* 23 (2011) 3202–3210.
- [57] Y.M. Shi, X.C. Dong, P. Chen, J.L. Wang, L.J. Li, *Phys. Rev. B: Condens. Matter* 79 (2009), 115402.
- [58] S. Ryu, L. Liu, S. Berciaud, Y.J. Yu, H.T. Liu, P. Kim, G.W. Flynn, L.E. Brus, *Nano Lett.* 10 (2010) 4944–4951.
- [59] W.J. Fang, A.L. Hsu, Y. Song, A.G. Birdwell, M. Amani, M. Dubey, M.S. Dresselhaus, T. Palacios, J. Kong, *ACS Nano* 8 (2014) 6491–6499.
- [60] X.M. Li, D. Xie, H. Park, T.H. Zeng, K.L. Wang, J.Q. Wei, M.L. Zhong, D.H. Wu, J. Kong, H.W. Zhu, *Adv. Energy Mater.* 3 (2013) 1029–1034.
- [61] Z.G. Cheng, Q.Y. Zhou, C.X. Wang, Q.A. Li, C. Wang, Y. Fang, *Nano Lett.* 11 (2011) 767–771.
- [62] Y.C. Lin, C.C. Lu, C.H. Yeh, C.H. Jin, K. Suenaga, P.W. Chiu, *Nano Lett.* 12 (2012) 414–419.
- [63] K. Kumar, Y.S. Kim, E.H. Yang, *Carbon* 65 (2013) 35–45.
- [64] E.Z. Shi, H.B. Li, L. Yang, L.H. Zhang, Z. Li, P.X. Li, Y.Y. Shang, S.T. Wu, X.M. Li, J.Q. Wei, K.L. Wang, H.W. Zhu, D.H. Wu, Y. Fang, A.Y. Cao, *Nano Lett.* 13 (2013) 1776–1781.
- [65] J.W. Suk, W.H. Lee, J. Lee, H. Chou, R.D. Piner, Y.F. Hao, D. Akinwande, R.S. Ruoff, *Nano Lett.* 13 (2013) 1462–1467.
- [66] D.L. Duong, G.H. Han, S.M. Lee, F. Gunes, E.S. Kim, S.T. Kim, H. Kim, Q.H. Ta, K.P. So, S.J. Yoon, S.J. Chafe, Y.W. Jo, M.H. Park, S.H. Chafe, S.C. Lim, J.Y. Choi, Y.H. Lee, *Nature* 490 (2012) 235–240.
- [67] K.K. Kim, A. Reina, Y.M. Shi, H. Park, L.J. Li, Y.H. Lee, J. Kong, *Nanotechnology* 21 (2010), 285205.
- [68] S. Oh, B.J. Kim, J. Kim, *Phys. Status Solidi RRL* 8 (2014) 441–444.
- [69] D.H. Shin, J.M. Kim, C.W. Jang, J.H. Kim, S. Kim, S.H. Choi, *J. Appl. Phys.* 113 (2013), 064305.
- [70] Y. Song, W.J. Fang, A.L. Hsu, J. Kong, *Nanotechnology* 25 (2014), 395701.
- [71] S. Tongay, K. Berke, M. Lemaitre, Z. Nasrollahi, D.B. Tanner, A.F. Hebard, B.R. Appleton, *Nanotechnology* 22 (2011), 425701.
- [72] T.-H. Han, Y. Lee, M.-R. Choi, S.-H. Woo, S.-H. Bae, B.H. Hong, J.-H. Ahn, T.-W. Lee, *Nat. Photonics* 6 (2012) 105–110.
- [73] H. Park, J.A. Rowehl, K.K. Kim, V. Bulovic, J. Kong, *Nanotechnology* 21 (2010), 505204.
- [74] I. Khrapach, F. Withers, T.H. Bointon, D.K. Polyushkin, W.L. Barnes, S. Russo, M.F. Craciun, *Adv. Mater.* 24 (2012) 2844–2849.
- [75] T.H. Bointon, I. Khrapach, R. Yakimova, A.V. Shytov, M.F. Craciun, S. Russo, *Nano Lett.* 14 (2014) 1751–1755.
- [76] W.Z. Bao, J.Y. Wan, X.G. Han, X.H. Cai, H.L. Zhu, D.H. Kim, D.K. Ma, Y.L. Xu, J.N. Munday, H.D. Drew, M.S. Fuhrer, L.B. Hu, *Nat. Commun.* 5 (2014).
- [77] S. Wang, P.K. Ang, Z. Wang, A.L.L. Tang, J.T.L. Thong, K.P. Loh, *Nano Lett.* 10 (2009) 92–98.
- [78] Z.Y. Yin, S.X. Wu, X.Z. Zhou, X. Huang, Q.C. Zhang, F. Boey, H. Zhang, *Small* 6 (2010) 307–312.
- [79] H. Feng, R. Cheng, X. Zhao, X. Duan, J. Li, *Nat. Commun.* 4 (2013) 1539.
- [80] H.A. Becerril, J. Mao, Z. Liu, R.M. Stoltenberg, Z. Bao, Y. Chen, *ACS Nano* 2 (2008) 463–470.
- [81] W.G. Townsend, *IEEE J. Solid-State Electr. Devices* 2 (1978) S31–S34.
- [82] X.M. Li, H.W. Zhu, K.L. Wang, A.Y. Cao, J.Q. Wei, C.Y. Li, Y. Jia, Z. Li, X. Li, D.H. Wu, *Adv. Mater.* 22 (2010) 2743–2750.
- [83] Y.M. Shi, K.K. Kim, A. Reina, M. Hofmann, L.J. Li, J. Kong, *ACS Nano* 4 (2010) 2689–2694.
- [84] X.H. An, F.Z. Liu, Y.J. Jung, S. Kar, *Nano Lett.* 13 (2013) 909–916.
- [85] K. Ihm, J.T. Lim, K.J. Lee, J.W. Kwon, T.H. Kang, S. Chung, S. Bae, J.H. Kim, B.H. Hong, G.Y. Yeom, *Appl. Phys. Lett.* 97 (2010), 032113.
- [86] X.C. Miao, S. Tongay, M.K. Petterson, K. Berke, A.G. Rinzler, B.R. Appleton, A.F. Hebard, *Nano Lett.* 12 (2012) 2745–2750.
- [87] X.M. Li, D. Xie, H. Park, M. Zhu, T.H. Zeng, K.L. Wang, J.Q. Wei, D.H. Wu, J. Kong, H.W. Zhu, *Nanoscale* 5 (2013) 1945–1948.
- [88] T.X. Cui, R.T. Lv, Z.H. Huang, S.X. Chen, Z.X. Zhang, X. Gan, Y. Jia, X.M. Li, K.L. Wang, D.H. Wu, F.Y. Kang, *J. Mater. Chem. A* 1 (2013) 5736–5740.
- [89] Y.X. Lin, X.M. Li, D. Xie, T.T. Feng, Y. Chen, R. Song, H. Tian, T.L. Ren, M.L. Zhong, K.L. Wang, H.W. Zhu, *Energy Environ. Sci.* 6 (2013) 108–115.
- [90] X. An, F. Liu, S. Kar, *Carbon* 57 (2013) 329–337.
- [91] Y. Song, X.M. Li, C. Mackin, X. Zhang, W.J. Fang, T. Palacios, H.W. Zhu, J. Kong, *Nano Lett.* 15 (2015) 2104–2110.
- [92] W. Regan, S. Byrnes, W. Gannett, O. Ergen, O. Vazquez-Mena, F. Wang, A. Zettl, *Nano Lett.* 12 (2012) 4300–4304.
- [93] R. Hezel, *Sol. Energy Mater. Sol. Cells* 74 (2002) 25–33.
- [94] L. Leonat, M.S. White, E.D. Glowacki, M.C. Scharber, T. Zillger, J. Ruhlmann, A. Hubler, N.S. Sariciftci, *J. Phys. Chem. C* 118 (2014) 16813–16817.
- [95] H. Park, S. Chang, X. Zhou, J. Kong, T. Palacios, S. Gradečak, *Nano Lett.* 14 (2014) 5148–5154.
- [96] B. Kan, Q. Zhang, M.M. Li, X.J. Wan, W. Ni, G.K. Long, Y.C. Wang, X. Yang, H.R. Feng, Y.S. Chen, *J. Am. Chem. Soc.* 136 (2014) 15529–15532.
- [97] Z.C. He, C.M. Zhong, S.J. Su, M. Xu, H.B. Wu, Y. Cao, *Nat. Photonics* 6 (2012) 591–595.
- [98] J. Kettle, H. Waters, M. Horie, S.W. Chang, *J. Phys. D: Appl. Phys.* 45 (2012), 125102.
- [99] H. Park, Y.M. Shi, J. Kong, *Nanoscale* 5 (2013) 8934–8939.
- [100] Y. Wang, X.H. Chen, Y.L. Zhong, F.R. Zhu, K.P. Loh, *Appl. Phys. Lett.* 95 (2009), 063302.
- [101] Y. Wang, S.W. Tong, X.F. Xu, B. Ozyilmaz, K.P. Loh, *Adv. Mater.* 23 (2011) 1514–1518.
- [102] J.P. Lock, S.G. Im, K.K. Gleason, *Macromolecules* 39 (2006) 5326–5329.
- [103] H. Park, R.M. Howden, M.C. Barr, V. Bulovic, K. Gleason, J. Kong, *ACS Nano* 6 (2012) 6370–6377.
- [104] H. Park, S. Chang, M. Smith, S. Gradečak, J. Kong, *Sci. Rep. (UK)* 3 (2013), 1581.
- [105] H. Park, P.R. Brown, V. Bulovic, J. Kong, *Nano Lett.* 12 (2012) 133–140.
- [106] Y.Y. Lee, K.H. Tu, C.C. Yu, S.S. Li, J.Y. Hwang, C.C. Lin, K.H. Chen, L.C. Chen, H.L. Chen, C.W. Chen, *ACS Nano* 5 (2011) 6564–6570.
- [107] Z.K. Liu, J.H. Li, Z.H. Sun, G.A. Tai, S.P. Lau, F. Yan, *ACS Nano* 6 (2012) 810–818.
- [108] Z.K. Liu, J.H. Li, F. Yan, *Adv. Mater.* 25 (2013) 4296–4301.
- [109] S.W. Tong, Y. Wang, Y. Zheng, M.F. Ng, K.P. Loh, *Adv. Funct. Mater.* 21 (2011) 4430–4435.
- [110] H. Park, J. Kong, *Adv. Energy Mater.* 4 (2014), 1301280.
- [111] X. Wang, L.J. Zhi, K. Mullen, *Nano Lett.* 8 (2008) 323–327.
- [112] H. Bi, S.R. Sun, F.Q. Huang, X.M. Xie, M.H. Jiang, *J. Mater. Chem.* 22 (2012) 411–416.
- [113] P. Dong, Y. Zhu, J. Zhang, F. Hao, J.J. Wu, S.D. Lei, H. Lin, R.H. Hauge, J.M. Tour, J. Lou, *J. Mater. Chem. A* 2 (2014) 20902–20907.
- [114] E. Yablonovitch, O.D. Miller, S.R. Kurtz, 2012 38th IEEE Photovoltaic Specialists Conference (PVSC), 2012, pp. 1556–1559.
- [115] W.J. Jie, F.G. Zheng, J.H. Hao, *Appl. Phys. Lett.* 103 (2013), 233111.

- [116] X. Li, W. Chen, S. Zhang, Z. Wu, P. Wang, Z. Xu, H. Chen, W. Yin, H. Zhong, S. Lin, *Nano Energy* 16 (2015) 310–319.
- [117] T.Q. Lin, F.Q. Huang, J. Liang, Y.X. Wang, *Energy Environ. Sci.* 4 (2011) 862–865.
- [118] N.J. Jeon, J.H. Noh, W.S. Yang, Y.C. Kim, S. Ryu, J. Seo, S.I. Seok, *Nature* 517 (2015) 476–480.
- [119] H.P. Zhou, Q. Chen, G. Li, S. Luo, T.B. Song, H.S. Duan, Z.R. Hong, J.B. You, Y.S. Liu, Y. Yang, *Science* 345 (2014) 542–546.
- [120] P. You, Z. Liu, Q. Tai, S. Liu, F. Yan, *Adv. Mater.* 27 (2015) 3632–3638.
- [121] J. Wu, M. Agrawal, H.A. Becerril, Z. Bao, Z. Liu, Y. Chen, P. Peumans, *ACS Nano* 4 (2009) 43–48.
- [122] T. Sun, Z.L. Wang, Z.J. Shi, G.Z. Ran, W.J. Xu, Z.Y. Wang, Y.Z. Li, L. Dai, G.G. Qin, *Appl. Phys. Lett.* 96 (2010), 133301.
- [123] N. Li, S. Oida, G.S. Tulevski, S.-J. Han, J.B. Hannon, D.K. Sadana, T.-C. Chen, *Nat. Commun.* 4 (2013), 2294.
- [124] J. Meyer, P.R. Kidambi, B.C. Bayer, C. Weijtens, A. Kuhn, A. Centeno, A. Pesquera, A. Zurutuza, J. Robertson, S. Hofmann, *Sci. Rep.* 4 (2014), 5380.
- [125] B.-J. Kim, G. Yang, H.-Y. Kim, K.H. Baik, M.A. Mastro, J.K. Hite, C.R. Eddy, F. Ren, S.J. Pearton, J. Kim, *Opt. Express* 21 (2013) 29025–29030.
- [126] D.-H. Youn, Y.-J. Yu, H. Choi, S.-H. Kim, S.-Y. Choi, C.-G. Choi, *Nanotechnology* 24 (2013) 075202.
- [127] X. An, F. Liu, Y.J. Jung, S. Kar, *Nano Lett.* 13 (2013) 909–916.
- [128] J. Kim, S.S. Joo, K.W. Lee, J.H. Kim, D.H. Shin, S. Kim, S.-H. Choi, *ACS Appl. Mater. Interfaces* 6 (2014) 20880–20886.
- [129] Y.-H. Kim, S.-H. Kwon, J.M. Lee, M.-S. Hwang, J.-H. Kang, W.I. Park, H.-G. Park, *Nat. Commun.* 3 (2012) 1123.
- [130] E.J.H. Lee, K. Balasubramanian, R.T. Weitz, M. Burghard, K. Kern, *Nat. Nanotechnol.* 3 (2008) 486–490.
- [131] F.N. Xia, V. Perebeinos, Y.M. Lin, Y.Q. Wu, P. Avouris, *Nat. Nanotechnol.* 6 (2011) 179–184.
- [132] M.S. Lee, K. Lee, S.Y. Kim, H. Lee, J. Park, K.H. Choi, H.K. Kim, D.G. Kim, D.Y. Lee, S. Nam, J.U. Park, *Nano Lett.* 13 (2013) 2814–2821.
- [133] B. Deng, P.C. Hsu, G.C. Chen, B.N. Chandrashekar, L. Liao, Z. Ayitimuda, J.X. Wu, Y.F. Guo, L. Lin, Y. Zhou, M. Aisijiang, Q. Xie, Y. Cui, Z.F. Liu, H.L. Peng, *Nano Lett.* 15 (2015) 4206–4213.
- [134] Y. Zhu, L. Li, C.G. Zhang, G. Casillas, Z.Z. Sun, Z. Yan, G.D. Ruan, Z.W. Peng, A.R.O. Raji, C. Kittrell, R.H. Hauge, J.M. Tour, *Nat. Commun.* 3 (2012), 1225.
- [135] S. Iijima, *Nature* 354 (1991) 56–58.
- [136] T.W. Ebbesen, P.M. Ajayan, *Nature* 358 (1992) 220–222.



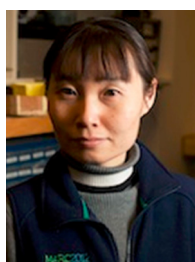
Yi Song received his B.S. in electrical engineering from the University of California Berkeley in 2011. He is currently pursuing his Ph.D. degree in electrical engineering at the Massachusetts Institute of Technology under Professor Kong. His research involves using graphene as transparent electrodes in optoelectronic devices with a focus on polymer and other thin-film solar cells.



Wenjing Fang joined Professor Kong's group in August 2010 as a Ph.D. candidate in Electrical Engineering. She received her B.Eng. in Materials Science and Engineering department from Nanyang Technological University. Her current research focuses on the synthesis and characterization of two dimensional materials such as graphene and hexagonal boron nitride.



Roberto Brenes an undergraduate in the department of Electrical Engineering and Computer Science at MIT. His research interests include the optical and electrical characterization of emerging photovoltaic devices. He is currently working on the spectroscopy of perovskites for use in solar cells.



Professor Jing Kong is a principal investigator in the department of Electrical Engineering and Computer Science at the Massachusetts Institute of Technology. She received her B.S. in chemistry from Peking University in 1997 and her Ph.D. in chemistry from Stanford University in 2002. She joined the MIT faculty in 2004. The current research activity in her group involves synthesis, characterization of graphene and related nano-materials, investigation of their electronic and optical properties and developing their applications.